The single-phase multiferroic oxides: from bulk to thin film

2005 J. Phys.: Condens. Matter 17 R803

(http://iopscience.iop.org/0953-8984/17/30/R01)

INSTITUTE OF PHYSICS PUBLISHING JOURNAL OF PHYSICS: CONDENSED MATTER

J. Phys.: Condens. Matter **17** (2005) R803–R832 doi:10.1088/0953-8984/17/30/R01

TOPICAL REVIEW

The single-phase multiferroic oxides: from bulk to thin film

W Prellier, M P Singh and P Murugavel

Laboratoire CRISMAT, CNRS UMR 6508, ENSICAEN, 6 Boulevard du Maréchal Juin, F-14050 Caen Cedex, France

E-mail: prellier@ensicaen.fr

Received 22 February 2005, in final form 7 June 2005
Published 15 July 2005
Online at stacks.iop.org/JPhysCM/17/R803

Abstract

Complex perovskite oxides exhibit a rich spectrum of properties, including magnetism, ferroelectricity, strongly correlated electron behaviour, superconductivity and magnetoresistance, which have been research areas of great interest among the scientific and technological community for decades. There exist very few materials which exhibit multiple functional properties; one such class of materials is called the multiferroics. Multiferroics are interesting because they exhibit simultaneously ferromagnetic and ferroelectric polarizations and a coupling between them. Due to the nontrivial lattice coupling between the magnetic and electronic domains (the magnetoelectric effect), the magnetic polarization can be switched by applying an electric field; likewise the ferroelectric polarization can be switched by applying a magnetic field. As a consequence, multiferroics offer rich physics and novel devices concepts, which have recently become of great interest to researchers. In this review article the recent experimental status, for both the bulk single phase and the thin film form, has been presented. Current studies on the ceramic compounds in the bulk form including $Bi(Fe, Mn)O_3$, $REMnO_3$ and the series of $REMn_2O_5$ single crystals (RE = rare earth) are discussed in the first section and a detailed overview on multiferroic thin films grown artificially (multilayers and nanocomposites) is presented in the second section.

(Some figures in this article are in colour only in the electronic version)

Contents

1. Introduction 804
2. Bulk single phase 805
   2.1. Bi-based compounds 805
   2.2. Other perovskites and related materials: $REMnO_3$ compounds (RE = Y, Ho, Er, Tm, Yb, Lu) 809
   2.3. $REMn_2O_5$ 814

3. Thin films 817
3.1. Single-phase compound 817
3.2. Artificial multimaterials 824
4. Conclusion 829
Acknowledgments 829
References 829

1. Introduction

Magnetic and ferroelectric materials are time-honoured research subjects which have led to new discoveries, both scientific and technological. Due to their interesting physical, chemical and mechanical properties, these materials have been used to realize a vast number of devices ranging from giant devices like electrical transformers to tiny devices like sensors, used in integrated circuits or as a storage devices. Furthermore, these materials are likely to offer new kinds of devices and functionality, because of their size-dependent physical and chemical properties, which have motivated a lot of current research activity in the area of ferroelectric and magnetic materials. For example, by coupling the elastic and nanometric magnetic domains, one can realize several novel devices, e.g. break junctions and ballistic electrons [1–4].

Ferromagnetic materials possess spontaneous magnetization (i.e. magnetic polarization) and which can be switched by an applied magnetic field. For decades, enormous activity has been concentrated on the search for new ferromagnetic materials and controlling the properties of these materials through their structure and size. Similarly, ferroelectric materials possess a spontaneous electric polarization, the direction of which can be switched with an applied electric field. In fact, in the case of ferroelectric materials, the 'ferro' part of the name arises from their electrical properties which are similar to the magnetic properties of iron-based magnetic materials; most of them, however, are not ferrous, since they do not contain iron. Ferroelectrics are used to make capacitors with high dielectric constant materials, and also have applications in nonvolatile data storage etc. These phenomena, i.e. ferroelectricity and ferromagnetism, derive from the fact that the electrons possess charge and spin. Depending on the surroundings, a material may have an electric polarization or a magnetic polarizations. A few materials possess both ferroelectric and magnetic polarizations, and are called multiferroic [5]. Thus, the multiferroics are materials that are simultaneously ferromagnetic and ferroelectric in the same phase and a coupling between them. As a consequence, they have a spontaneous magnetization that can be switched by an applied electric field and a spontaneous electrical polarization that can be switched by an applied magnetic field [6]. Due to the coupling between ferroelectric and magnetic domains, multiferroics are likely to offer a whole range of new applications and phenomena. First, the ability to couple to either the electric or the magnetic polarization allows an additional degree of freedom in device design. Other applications include multiple-state memory elements, in which data are stored both in the electric and magnetic polarizations, and novel memory media, which might allow the writing of a ferroelectric data bit and reading of the magnetic field generated by association. Aside from the potential applications, the fundamental physics of multiferroic materials is rich and fascinating.

Hitherto, there have been very few multiferroics existing in nature or synthesized in the laboratory. The first multiferroic material which was discovered was nickel iodine boracite, ($Ni_3B_2O_{13}I$) [7]. This discovery was followed by the synthesis of several multiferroic boracite compounds, all of which have complex structures with many atoms per formula unit and more than one formula unit per unit cell. The large number of inter-ionic interactions in these materials prevented isolation of the essential factors causing multiferroicity and the nature of

the coupling between the magnetic and electric polarization, and structural order parameters. Nickel iodine boracite can be thought of as the 'Rochelle salt' of magnetic ferroelectrics—invaluable for demonstrating proof of concept, but unlikely to find wide applicability or to contribute to our increased understanding in the field.

The search for other multiferroics began in Russia as early as the 1950s, with the replacement of some of the d^0 B cations in ferroelectric perovskite oxides by magnetic d^n cations [8]. The first synthetic multiferroic material, $(1 - x)$ $PbFe_{0.66}W_{0.33}O_3$–$xPbMg_{0.5}W_{0.5}O_3$ [9], was produced at the beginning of the 1960s. In this case, Mg^{2+} and W^{6+} ions were diamagnetic and caused ferroelectricity whereas d^5 Fe^{3+} ions are responsible for the magnetic ordering. Other examples include B site disordered $Pb_2(Co, W)O_6$ [10], which is ferroelectric and ferromagnetic, B site disordered Pb_2FeTaO_6, which is ferroelectric and antiferromagnetic, and $Pb_2(FeTa)O_6$ [11, 12], which are both ferroelectric and antiferromagnetic with weak ferromagnetism around 10 K. As a result of the dilution of the magnetic ions, these materials all have rather low Curie or Néel temperatures.

In the past few years, there has been renewed interest in studying the perovskite-based multiferroic materials, such as rare earth manganates $TbMn_2O_5$, $YMnO_3$, $BiMnO_3$, which have higher Curie temperatures (except for $YMnO_3$ which is antiferromagnetic) and large magnetoelectric effects. Furthermore, recently efforts have been made to synthesize the new multiferroic in the form of a thin film, by employing ferroelectric and magnetic compounds to make a nanocomposite or a superlattice or a multilayer structure. The aim of this review article is to introduce the current materials, both in the bulk (as a single phase) and thin film forms, which are under study and the various approaches which have been followed to synthesize the new compounds which behave as multiferroics. For the sake of clarity we have divided the article into two major sections. The first section deals with bulk materials and the second section deals with materials in thin film form. In this review article, we have deliberately focused on single-phase multiferroics (bulk and thin film) and have not reviewed the results on layered composites [13–15].

2. Bulk single phase

From the end of the 1990s, significant progress has been made in synthesizing and characterizing various oxides, which show the multiferroism property at high temperatures [16–18]. This search led to the study of various oxides in the bulk, for example Bi-based compounds, namely $BiMnO_3$ or $BiFeO_3$. Further several attempts have been made to enhance the magnetoelectric coupling in these oxides through Bi site substitutions. Other compounds which are also under investigation include the rare earth-based perovskites. In the present section, we will describe the study of Bi-based compounds and this will be followed by a description of the study of rare earth manganites. At the end of this section, we will present the work on $REMn_2O_5$-type compounds (RE = rare earth).

2.1. Bi-based compounds

$BiMnO_3$ was studied in the form of bulk material because recent theoretical calculations suggest that this perovskite has only a simple B site cation, and it is likely to be both ferromagnetic and ferroelectric because of the covalent bonding between bismuth and oxygen atoms [17, 18].

$BiMnO_3$, like $YMnO_3$, is a compound that has been intensively studied because of its multiferroic properties, both theoretically and experimentally, and it displays a ferromagnetic transition temperature (T_C) at around 105 K and a ferroelectric transition temperature (T_E) at 750 K [19]. The structure of the ferromagnetic $BiMnO_3$ (Curie temperature T_C =

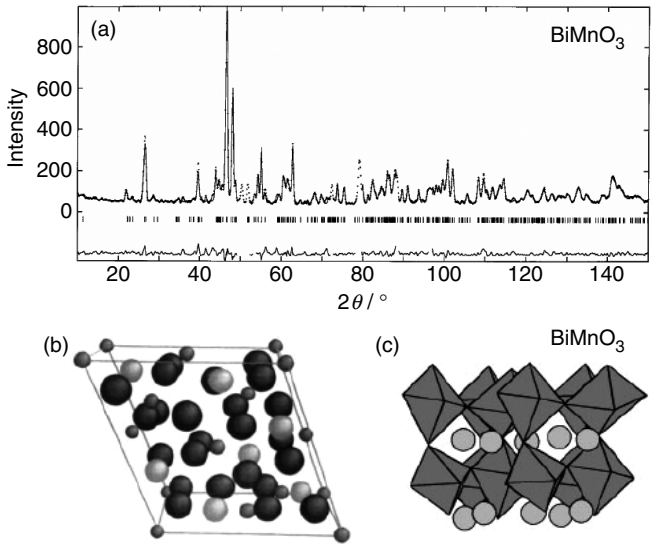

Figure 1. (a) The observed (dots) and calculated (line) profiles of $BiMnO_3$ after the final refinement. Schematic illustrations of the crystal structure of $BiMnO_3$. (b) Unit cell view: large, O^{2-}; medium, Bi^{3+}; small, Mn^{3+}. (c) A part of the crystal structure is shown on the basis of the perovskite unit. MnO_6 octahedra and bismuth cations are represented. Adapted from [22, 23].

105 K) [20, 21], synthesized at high pressure (6 GPa), was determined by electron diffraction and neutron powder diffraction studies (figure 1) [22, 23]. These studies show that $BiMnO_3$ possesses a distorted perovskite (figure 1) structure, having monoclinic symmetry with space group $C2$ and lattice parameters $a = 9.5323(6)$ Å, $b = 5.6064(3)$ Å, $C = 9.8535(7)$ Å and $\beta = 110.667(5)^\circ$ [22, 23]. The distortion is caused by a polarized Bi $6s^2$ lone pair as calculated from first-principles electronic structure calculations [24]. Every trivalent manganese cation reveals Jahn–Teller distortion, and ordering of a vacant $d_{x^2-y^2}$ orbital is suggested to play an important role for the ferromagnetism [22], confirming the calculations indicating that the Mn 3d states experience orbital ordering [25]. From these investigations, Shishidou *et al* found that the lattice instability to the off-centred displacement is due to the strong covalent bonding between Bi 6p and O 2p states [26].

Kimura *et al* [27] have found a ferroelectric transition temperature in the range of 750–770 K which has been attributed to a centrosymmetric-to-noncentrosymmetric structural transition, which indicates the presence of ferroelectricity in the system. A large magnetocapacitance effect is also observed near the ferromagnetic transition temperature (see figure 2). These features are attributed to the inherent coupling between the ferroelectric and ferromagnetic orders in the multiferroic system [27]. This coupling was in fact predicted from the molecular field approximation [28].

Various studies suggested that the statistical distribution of Fe^{3+} ions with 4+ ions in the octahedra or the creation of lattice defects can lead to bulk magnetization and ferromagnetism [29, 30]. Thus, it was interesting to replace Fe^{3+} by Mn^{4+} in $BiFeO_3$ in order to improve the magnetic characteristics. To see such an effect, Palkar *et al* have studied the substitution of Mn in the $Bi_{0.9}La_{0.1}Fe_{1-x}Mn_xO_3$ ($0 \leqslant x \leqslant 0.5$) bulk compound [31]. In that case, the small amount of La is only used to stabilize the distorted $BiMnO_3$ perovskite and does not affect the ferroelectric properties [32]. It is not possible to obtain a single phase above $x = 0.5$ content of Fe (see figure 3) which probably indicates a saturation threshold,

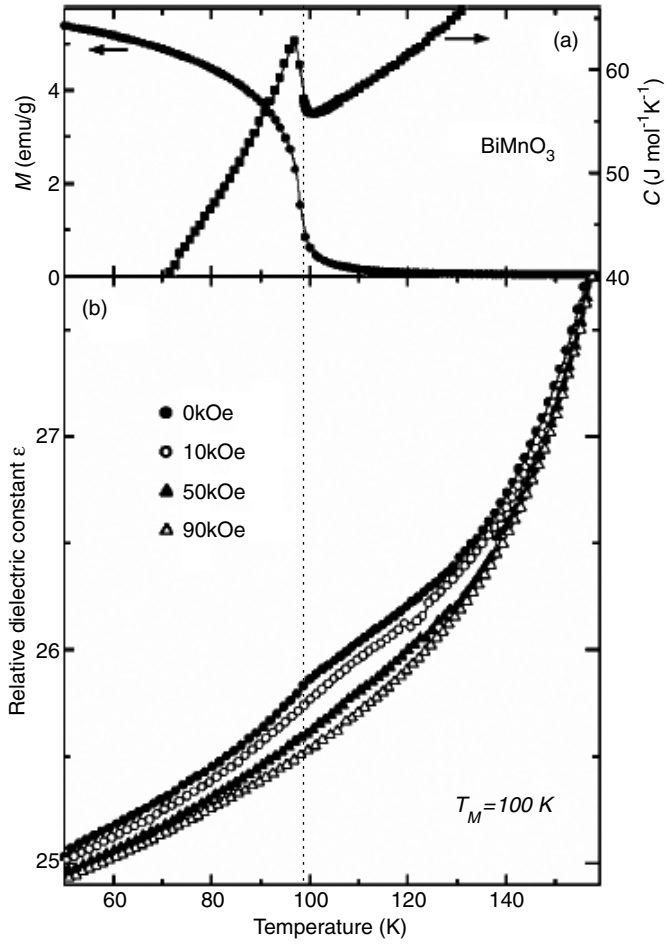

Figure 2. Temperature dependence of (a) the magnetization at 100 Oe, the specific heat and (b) the real part of the relative dielectric constant of $BiMnO_3$ at selected magnetic fields in the vicinity of the magnetic transition. A steep rise of magnetization toward lower temperature and an anomaly of the specific heat at $T_M = 100$ K correspond to the onset of ferromagnetic ordering. Adapted from [27].

at least for classical solid state routes. In addition, they observed that, with the increase in Mn content, there is a decrease in the a and c lattice constants leading to a contraction of the unit cell volume (probably due to the smaller ionic radius of Mn^{4+} as compared to Fe^{3+}). Since the cell volume contraction is isotropic, the lattice distortion (c/a) remains the same. Their study showed that the ferroelectric transition temperature (T_E) is independent of the Mn doping content and it is also observed that the presence of Mn does not affect the loss tangent ($\tan\delta = 0.077$) of the samples. On the contrary, with increase in Mn content, a small but linear enhancement in the magnetization is observed and the sample with $x = 0.5$ exhibits a remnant magnetization.

The achievement of $BiFeO_3$ as a single phase was possible, by leaching the impurity phase out with dilute nitric acid [33]. The $BiFeO_3$ compound crystallizes in a hexagonal structure (space group $R3c$) with lattice parameters $a = 5.5799$ Å and $c = 13.8670$ Å [34, 35]. It exhibits an antiferromagnetic behaviour with a relatively high Néel temperature ($T_N =$

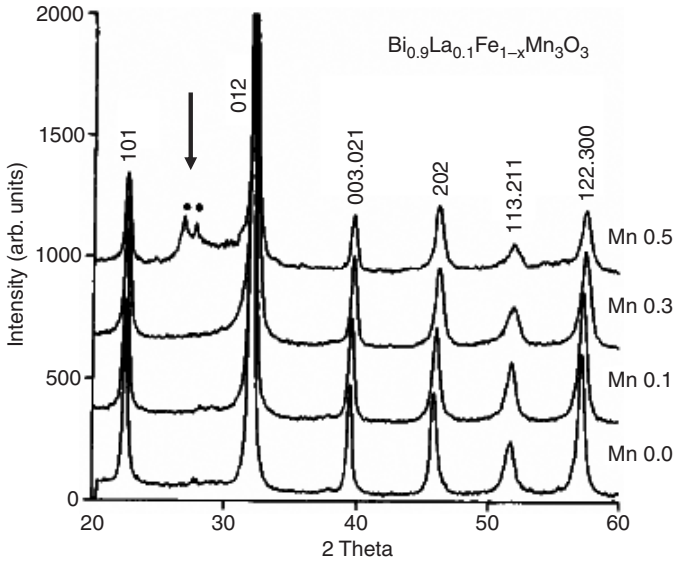

Figure 3. XRD patterns for $Bi_{0.9}La_{0.1}Fe_{1-x}Mn_xO_3$ ($0 < x < 0.5$) bulk samples. ● indicates the presence of impurity phase for $x = 0.5$ (see the arrow). Adapted from [31].

380 °C) and a ferroelectric behaviour with high Curie temperature ($T_C = 810$ °C). Its weak ferromagnetism at room temperature is due to a residual moment from the canted spin structure [36]. Single-phase ferromagnet $BiFeO_3$ ceramics with high resistivity were thus synthesized by a rapid liquid phase sintering technique [37]. Saturated ferroelectric hysteresis loops were observed at room temperature in the ceramics sintered at 880 °C for 450 s. The spontaneous polarization, remnant polarization and coercive field are 8.9 μC cm^{-2}, 4.0 μC cm^{-2} and 39 kV cm^{-1}, respectively, under an applied field of 100 kV cm^{-1}. Wang *et al* proposed that the formation of Fe^{2+} and an oxygen deficiency leading to the higher leakage can be greatly suppressed by a very high heating rate, short sintering period and liquid phase sintering technique [37].

In addition to the substitution of Fe at the Mn site, the solid solutions of $BiFeO_3$ with other ABO_3 perovskite have been the focused of study for a few groups. On this basis, single-phase polycrystalline samples of $Bi_{1-x}Nd_xFeO_3$ were prepared by the standard solid state reaction method [38]. X-ray diffraction studies were carried out on powder samples; these confirm that the materials have an orthorhombic crystal structure for $x = 1$, 0.8, 0.6 and 0.4, but not for $x = 0.2$ where the material crystallizes in a triclinic structure. This is a surprising result and a detailed structural refinement needs to be done to confirm this. The dielectric measurements were carried out on the samples as a function of frequency in the range 100 Hz–1 MHz at room temperature and also as a function of temperature in the range 300–750 K at certain fixed frequencies. A decrease in dielectric constant and loss with increasing frequency suggest a dielectric dispersion behaviour. The maximum is found for the $x = 0.2$ sample which corresponds to FeO_6 octahedra distortion [38]. Similarly, Palkar *et al* have synthesized $Bi_{0.9-x}Tb_xLa_{0.1}FeO_3$ [39]. On increasing the content of Tb, the structure remains unchanged, despite a small decrease of the volume of the unit cell (186 Å^3 for $x = 0$ and 183 Å^3 for $x = 0.075$). The Tb doped sample is ferromagnetic at room temperature whereas undoped $BiFeO_3$ is antiferromagnetic [33]. A saturated hysteresis loop is obtained at room temperature, confirming the ferroelectric behaviour of the $Bi_{0.9-x}Tb_xLa_{0.1}FeO_3$ compound. In

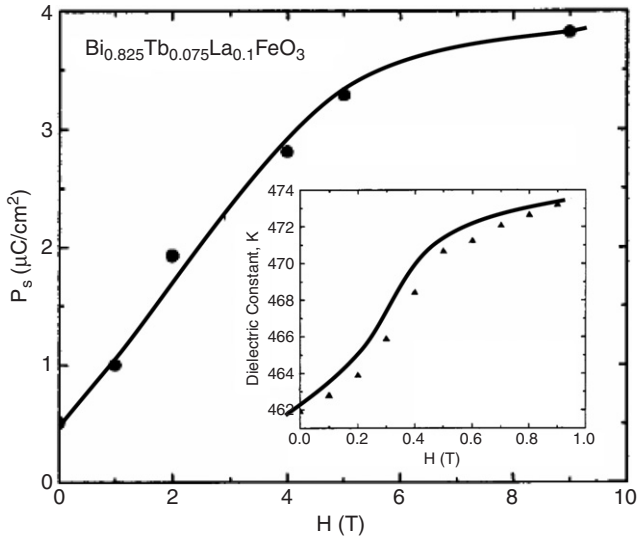

Figure 4. Room temperature saturation polarization versus magnetic field for a $Bi_{0.825}Tb_{0.075}La_{0.1}FeO_3$ ceramic sample. Inset: dielectric constant versus magnetic field for the same sample. Lines are guides for the eyes. Adapted from [39].

addition, the magnetoelectric coupling was evidenced by the increase of the dielectric constant with the increase of the applied magnetic field (figure 4) [39].

In conclusion, very few oxide materials exhibit the properties of both ferromagnetism and ferroelectricity [40, 41]. In fact only $BiMnO_3$, which can be made using high pressure synthesis, is a real multiferroic since $BiFeO_3$ is an antiferromagnet. For these reasons, it was necessary to look for other materials. The idea of using $REMnO_3$ and specifically $YMnO_3$ arose following the theoretical work [16]. In that study, Filippetti and Hill showed the fundamental role of the d electron occupation in preventing or favouring the simultaneous presence of magnetic and electric polarization. They also explained theoretically the coexistence of antiferromagnetism and ferroelectricity in the hexagonal phase of $YMnO_3$, which is ferroelectric along the *c* axis. This work aroused renewed interest in studying the ferroelectric/magnetic properties of hexagonal $YMnO_3$ and related compounds.

2.2. Other perovskites and related materials: $REMnO_3$ compounds (RE = Y, Ho, Er, Tm, Yb, Lu)

As demonstrated for $BiMnO_3$ and $BiFeO_3$ compounds, the properties of these perovskite compounds can be tailored by A site cation engineering, which is currently the focus of extensive research work; this has led to the study of various $REMnO_3$ perovskites as regards multiferroism. In the current section, we are focusing on the structure and properties of various rare earth perovskite manganites ($REMnO_3$). Usually, rare earth perovskite manganites compounds with RE = Y, Ho, Er, Tm, Yb, Lu, Sc exhibit hexagonal crystallographic structures, in contrast to those REs with larger ionic radius which exhibit orthorhombic perovskite structure. Structures of these rare earth compounds were well studied in the middle of the 20th century [42–46] and they have been recently revisited ($ErMnO_3$ [47], $YbMnO_3$ [48], $YMnO_3$ [49], $TbMnO_3$ [50] and $LuMnO_3$ [51]). With the reduction of the ionic radius of the A cation as one goes from Y to Lu, the orthorhombic (space group: *Pnma*) and the Jahn–Teller

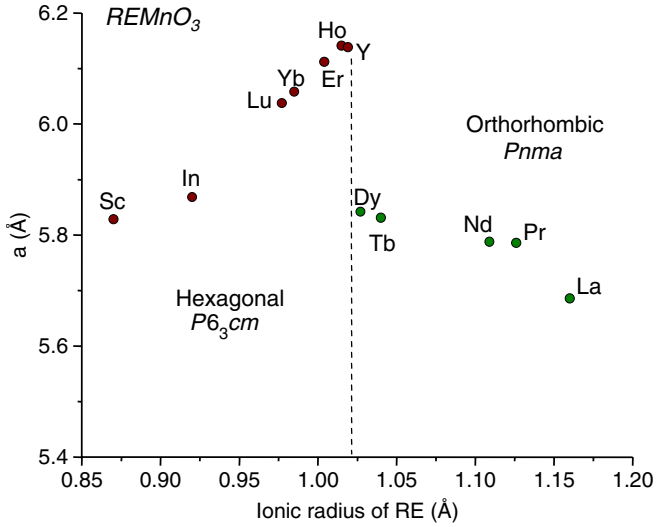

Figure 5. Evolution of the lattice structure in $REMnO_3$ as a function of the size of the rare earth (RE).

distorted perovskite structure become less stable and the structure of $REMnO_3$ often becomes hexagonal (space group: $P6_3cm$). The crossover is around Y/Ho (see figure 5). Moreover, some of the compounds exhibit both hexagonal and orthorhombic crystallographic structures, but the orthorhombic phase of these oxides had only been achieved by special synthesis routes, e.g. soft chemical means or thin film process [52]. Recent studies clearly demonstrate that the $REMnO_3$ with the trivalent rare earth ions having small ionic radius (A = Ho–Lu, Y, Sc), which possess stable hexagonal structures, can also be stabilized in the metastable orthorhombic $GdFeO_3$-type form [53]. As an example, $DyMnO_3$ can be stabilized both in hexagonal as well as in orthorhombic structure [54]. Generally the hexagonal manganites exhibit two kinds of ordering phenomena: magnetic ordering around 100 K and ferroelectric ordering around 900 K [55]. The ferroelectric properties can be traced to the noncentrosymmetric space group with a polar direction parallel to c axis, whereas the orthorhombic compounds form the basis for the colossal magnetoresistance (CMR) materials and they have been extensively studied in recent years, since their discovery, and these compounds exhibit the centrosymmetric space group, unlike the hexagonal structure, which is noncentrosymmetric—a key structural reason for materials exhibiting ferroelectricity.

The hexagonal manganite $YMnO_3$ and the Bi series compounds are other representative multiferroic materials exhibiting ferroelectricity and magnetism simultaneously (note that $YMnO_3$ exists as a cubic perovskite structure but does not exhibit ferroelectricity). Hexagonal $YMnO_3$ possesses the $P6_3cm$ space group with lattice parameters $a = 6.125$ Å and $c = 11.41$ Å at 290 K (figure 6) [44, 49]. Its structure consists of layers of two-dimensional connected distorted MnO_5 bipyramids separated by distorted layers of rare earths, leading to frustrated Mn^{3+}–O^{2-}–Mn^{3+} in-plane exchange paths and Mn^{3+}–O^{2-}–O^{2-}–Mn^{3+} interplane exchange paths [56]. Detailed study of the properties of $YMnO_3$ shows that it is an insulator [57] and exhibits ferroelectricity (spontaneous polarization close to 5.5 $\mu C\,cm^{-2}$) as well as antiferromagnetic properties, with a strong coupling between them [58]. Spatial maps of coupled antiferromagnetic and ferroelectric domains were thus imaged with optical second-harmonic generation [59]. Using this technique, Fiebig *et al* found that the coupling originates

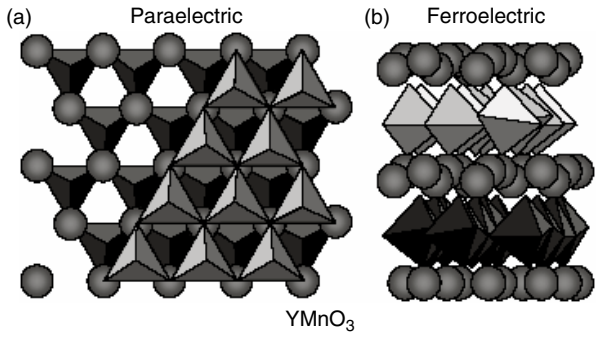

Figure 6. The crystal structure of $YMnO_3$ in the paraelectric and ferroelectric phases. The trigonal bipyramids depict MnO_5 polyhedra and the spheres represent Y ions. (a) The stacking of two consecutive MnO_5 layers and the sandwiched Y layer, looking down the *c* axis in the paraelectric phase. (b) A view of the ferroelectric phase from the perpendicular to the *c* axis, showing the layered nature of $YMnO_3$. Adapted from [61].

from an interaction between magnetic and electric domains walls, which led to a configuration that is dominated by the ferroelectromagnetic product of the order parameters. Note that these local interactions were also reported in the case of hexagonal $HoMnO_3$, where it is observed that the domain walls decrease the local magnetic symmetry, thus allowing magnetoelectric coupling between wall magnetization and ferroelectric polarization which modifies the dielectric function [60]. The origin of polarization in $YMnO_3$ (and thus ferroelectricity) is a consequence of the unusual Y site coordination and the triangular and layered MnO_5 network (see figure 6) [61]. As mentioned above, the crystal structure of ferroelectric-$YMnO_3$ is well studied but recent theoretical studies clearly demonstrate that there exist various possibilities for the rearrangement of the spins without losing the ferroelectricity, which leads to the possibility of various magnetic structure formations [62, 63]. Also focused efforts have been made to examine the thermal properties of $YMnO_3$ compound. The thermal conductivity of hexagonal $YMnO_3$ exhibits an isotropic suppression in the cooperative paramagnetic state, followed by a sudden increase upon magnetic ordering. This unprecedented behaviour without an associated static structural distortion probably originates from the strong dynamic coupling between acoustic phonons and low energy spin fluctuations in geometrically frustrated magnets. The replacement of magnetic Ho for Y at the ferroelectric active site results in an even larger effect, suggestive of a strong influence of multiferroicity [64]. As a consequence, several groups have focused their study on $HoMnO_3$ compounds. In this context, a re-entrant novel phase [65] is observed in the hexagonal ferroelectric $HoMnO_3$ in the presence of magnetic fields in the temperature range defined by a plateau of the dielectric constant anomaly. The plateau evolves with field from a narrow dielectric peak at the Mn spin rotation transition at 32.8 K in zero field. The anomaly appears both as a function of temperature and as a function of magnetic field without detectable hysteresis. This is attributed to the indirect coupling between the ferroelectric and antiferromagnetic orders, arising from an ferroelectric and antiferromagnetic domain wall effect [66]. A large magnetodielectric effect was observed in hexagonal $HoMnO_3$ at low temperature, where the dielectric constant (ϵ) can be tuned by an external magnetic field resulting in a decrease of up to 8% at 7 T. In addition to hexagonal $HoMnO_3$, orthorhombic $HoMnO_3$ has also been investigated. A remarkable increase (up to 60%) of the dielectric constant (figure 7) with the onset of magnetic order at 42 K in the metastable *orthorhombic* structures of $YMnO_3$ and $HoMnO_3$ was observed, which clearly demonstrates the existence of a strong magnetodielectric coupling in these compounds, similarly to previous reports [67].

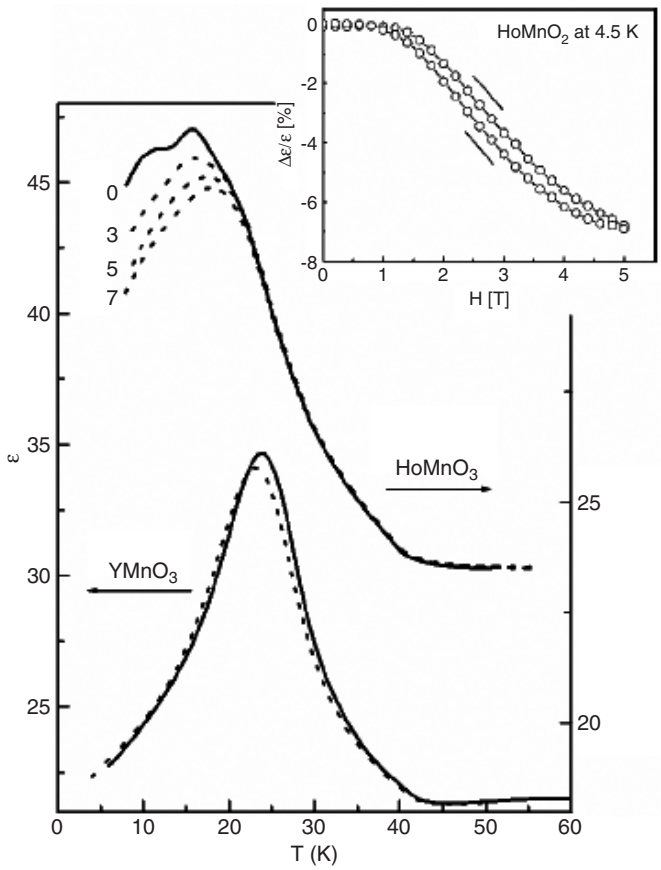

Figure 7. Magnetodielectric effect in $YMnO_3$ (full line: $H = 0$; dotted line: $H = 7$ T) and in $HoMnO_3$ (full line: $H = 0$; dotted lines: $H = 3, 5, 7$ T). Inset: the relative change of the dielectric constant as a function of the magnetic field for $HoMnO_3$ at 4.5 K. Adapted from [66].

Magnetic, dielectric and thermodynamic properties clearly show distinct anomalies at the onset of the incommensurate magnetic order and thermal hysteresis effects are observed around the lock-in transition temperature at which the incommensurate magnetic order locks into a temperature-independent wavevector. The Mn^{3+} spins and Ho^{3+} moments both contribute to the magnetodielectric coupling. By comparing the data for $YMnO_3$ and $HoMnO_3$, Lorenz *et al* have been able to separate the contributions coming from the coupling between the dielectric response and Mn and Ho magnetic moments [66]. Similar anomalies have also been observed at various magnetic transition temperatures in the hexagonal (Y/Ho)MnO_3; however the magnitude is small, in contrast with those for their orthorhombic counterparts [65]. Even the recently reported sharp peak of $\epsilon(T)$ at the spin rotation transition of hexagonal $HoMnO_3$, the strongest dielectric anomaly in hexagonal $REMnO_3$, does not exceed 45% in magnitude. The small response in the hexagonal structures of $YMnO_3$ and $HoMnO_3$, in contrast with their orthorhombic counterparts, can be explained by the existing ferroelectric order that forms well above room temperature in the hexagonal form. At the temperature of the magnetic transitions (100 K), the electrical polarization is rigid and any effects of magnetic order or magnetic fields on the dielectric constant are therefore small. Furthermore the 60% increase in the dielectric constant under applied magnetic field of the antiferromagnetic phase of the

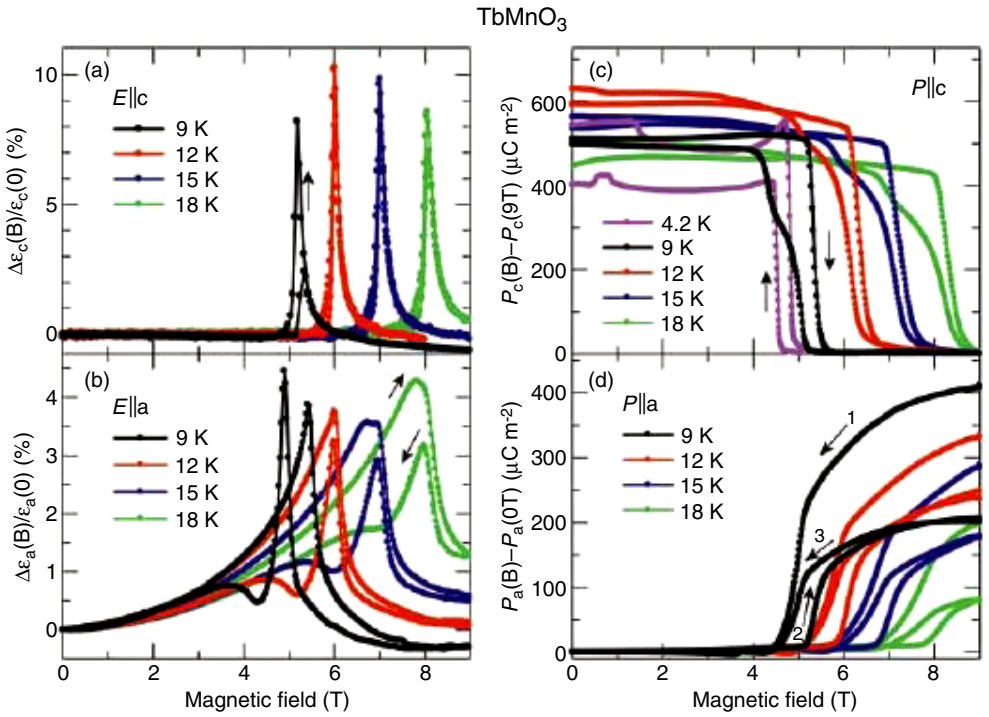

Figure 8. Magnetocapacitance and magnetoelectric effects in $TbMnO_3$. Magnetic field-induced change in the dielectric constant ((a) and (b)), electric polarization along the *c* and *a* axes, respectively ((c) and (d)), and magnetization at selected temperatures (e). Magnetic fields are applied along the *b* axis. The magnetic field dependence of the electric polarization was obtained by measurements of the magnetoelectric current, which were performed after poling the crystals. The data in (d) were collected after magnetic field cooling. The numbers in (d) denote the order of measurements at 9 K. Adapted from [69].

orthorhombic structure is very large in contrast those for with the hexagonal counterparts and this demonstrates that a huge magnetodielectric effect can be expected in the orthorhombic rare earth manganites.

Several groups have also recently investigated the structure and properties of $TbMnO_3$ [68]. The discovery of ferroelectricity in $TbMnO_3$ where the spin frustration causes sinusoidal antiferromagnetic ordering is an example of such materials. In this case, the modulated magnetic structure is accompanied by a magnetoelastically induced lattice modulation and the emergence of a spontaneous polarization. In this compound gigantic magnetoelectric and magnetocapacitance effects have been demonstrated (figure 8) and these were attributed to switching of the electric polarization induced by magnetic fields [69].

However, recent reports of the ferroelectric ordering temperatures in the multiferroic hexagonal $REMnO_3$ system are controversial in nature; i.e. transition temperatures varying between 900 and 1300 K are reported for the same material [55]. To elucidate the structural changes leading to ferroelectric distortions in hexagonal manganites, the irreducible representations of the distortions from the possible high temperature symmetry $P63/mmc$ to the low temperature symmetry $P63cm$ were calculated and the results showed that there are four different possible crystallographic orthogonal modes, of which only one allows a spontaneous electric polarization. Structural refinements and an accurate statistical analysis

of neutron powder diffraction data on $TmMnO_3$, based on this group theoretical analysis, reveal two phase transitions: one corresponds to a polar-to-nonpolar transition temperature at 1433(27) K, where the hexagonal bi-tetrahedra start to tilt, and another one corresponding to a ferroelectric distortion appears at $T_{FE} = 1050(50)$ K [55]. For RE = Lu, Yb, the tilt of the bi-tetrahedra and the buckling of the rare earth layers as well as the ferroelectric distortion were extrapolated to comparable temperatures [55].

Recent studies have also been focused on the $LuMnO_3$ compound. Souchkov *et al* have reported the optical conductivity, in the range of 10–45 000 cm^{-1} wavenumber, of single-crystal $LuMnO_3$ in the range of temperatures from 4 to 300 K. They found that a symmetry allowed on-site Mn d–d transition near 1.7 eV is observed to blueshift (∼0.1 eV) in the antiferromagnetic state due to Mn–Mn superexchange interactions. Similar anomalies are observed in the temperature dependence of the TO phonon frequencies which arise from spin–phonon interaction. They found that the observed anomaly in the temperature dependence of the quasi-static dielectric constant 0 below $T_N \sim 90$ K is overwhelmingly dominated by the phonon contributions [70]. Van Aken *et al* have studied the influence of antiferromagnetic ordering on the local dielectric moments of the MnO_5 and LuO_7 polyhedra by measuring neutron powder diffraction patterns of $LuMnO_3$ at temperatures near T_N. They have demonstrated that the magnetoelectric coupling is weak and can be understood on the basis of the fact that magnetic exchange coupling is predominantly in the *ab* plane of the MnO_5 trigonal bipyramids and the electric dipole moments originating in the LuO_7 polyhedra are oriented along the hexagonal *c* axis. Anomalies in the dielectric properties near T_N are thus caused by the geometric constraints between the MnO_5 and the LuO_7 polyhedra [71].

2.3. $REMn_2O_5$

The family $REMn_2O_5$ (RE = rare earth) was described first in 1964 [72, 73] but the multiferroism properties were discovered for $REMn_2O_5$ (RE = Y, Tb, Dy and Ho) only recently [74, 75]. An example of a typical structure is given in figure 9(a) for $TbMn_2O_5$. In this structure, the Mn^{3+} and Mn^{4+} ions occupy different crystallographic positions. While Mn^{4+} ions are octahedrally coordinated with oxygen, each Mn^{3+} ion is at the base centre of a square pyramid [76, 77]. All the phases with RE = La, Pr, Nd, Sm to Eu are isostructural [76] and the details of the lattice parameters are given in figure 9(b).

Most of the materials are obtained in the form of bulk ceramics. The polycrystalline powders have been obtained from precursors previously synthesized by dissolving A_2O_3 and $Mn(NO_3)_2{\cdot}4H_2O$ in citric acid [76] at high oxygen pressure or by using a sol–gel process [81]. But recently, several groups have been able to obtain single crystals (several mm in size) of $TbMn_2O_5$ [74, 78], $DyMn_2O_5$ [75, 79], $HoMn_2O_5$ [75], $GdMn_2O_5$ and $EuMn_2O_5$ [80] by utilizing the floating zone method. In general, the crystals are grown using B_2O_3–PbO–PbF_2 flux in a Pt crucible [74, 75, 78].

In $REMn_2O_5$ compounds, the ferroelectric transition is around 25–39 K and the antiferromagnetic transition temperature is in between 39 and 45 K [82]. The magnetic properties were measured and figure 10(a) shows an example of the magnetization versus magnetic field recorded at 3 K for (Tb, Dy, Ho)Mn_2O_5. From this figure, Hur *et al* [75] concluded that the magnetic easy axis is along the *a* axis for $TbMn_2O_5$ and along the *b* axis for (Dy, Ho)Mn_2O_5. The magnetic phase diagram was also investigated for $TbMn_2O_5$ by means of neutron diffraction [78] and Chapon *et al* found that the magnetic transitions (at 43, 33, 24 and 10 K) are associated with electric anomalies, confirming previous results of Hur *et al* [74, 75, 79]. Without a magnetic field applied, the dielectric constant starts to increase at 43 K (Néel temperature), exhibits a sharp peak at T_C (39 K) and shows step-like anomalies

(a)

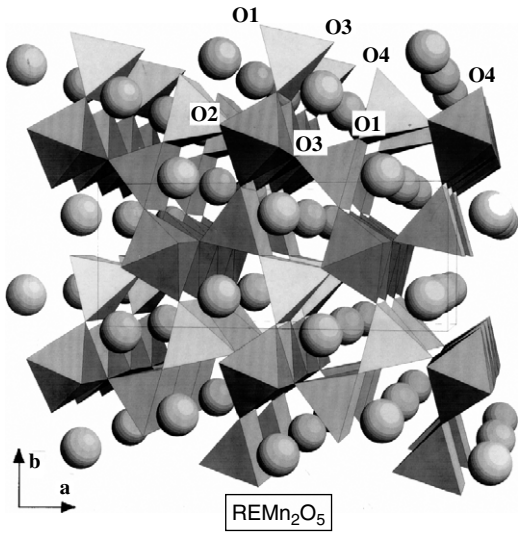

(b)

RE	a (Å)	b (Å)	c (Å)	V (Å)^3
La	7.6891(7)	8.7142(7)	5.7274(5)	383.76(9)
Pr	7.5583(9)	8.6481(9)	5.7119(6)	373.4(1)
Nd	7.5116(8)	8.6270(8)	5.7060(5)	369.76(9)
Sm	7.4332(7)	8.5872(7)	5.6956(5)	363.55(9)
Eu	7.3986(8)	8.5666(9)	5.6925(6)	360.8(1)

Figure 9. (a) Projection of the $REMn_2O_5$ structure, approximately along the *c* axis. Octahedra and tetragonal pyramids correspond to $Mn1O_6$ and $Mn2O_5$ units, respectively. The structure is orthorhombic (space group *Pbam*). Adapted from [76]. (b) Room temperature lattice parameters and volume of $REMn_2O_5$. Adapted from [76].

at 27 and 8 K. Hur *et al* suggested that these clear dielectric anomalies, occurring at each magnetic transition, undoubtedly indicate a significant spin–lattice coupling [75]. These three distinct ferroelectric transitions were clearly identify for $DyMn_2O_5$ [79]. For example, the zero-field lowest temperature (8 K) induced by the Dy moment ordering is a re-entrant pre-electric state but turned into a ferroelectric state with increasing field [79]. The most striking feature is the large change of the dielectric constant observed for $DyMn_2O_5$ under a magnetic field [75]. The dielectric constant exhibits a change of 109% at 3 K upon the application of a 7 T magnetic field. Similar behaviours are observed for $TbMn_2O_5$ and $HoMn_2O_5$ but the effect is smaller (20% for $TbMn_2O_5$ and 40% for $HoMn_2O_5$ at 9 T). The coupling between magnetic and dielectric properties was confirming for $DyMn_2O_5$ where a magnetic field modifies the ferroelectric state [79] (see figure 10(b)).

The dynamics of $EuMn_2O_5$ and $GdMn_2O_5$ crystals, showing magnetic and ferroelectric phase transitions with close transition temperatures (40 and 30 K for RE = Eu and Gd, respectively), were studied in the frequency and temperature ranges 20–300 GHz and 5–50 K, respectively. It was found that the magnetic resonance spectra of $GdMn_2O_5$ are characteristic

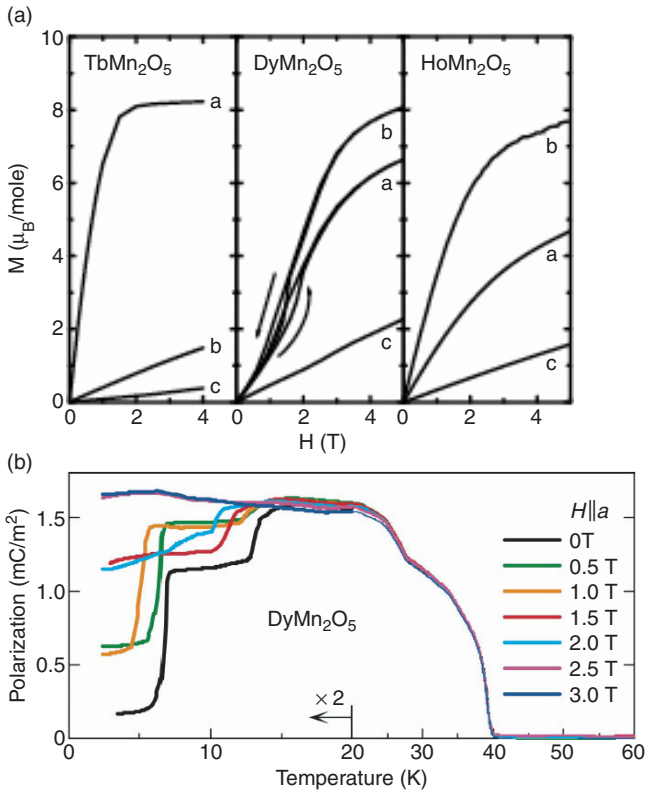

Figure 10. (a) Magnetization versus magnetic field at 3 K along the three principal crystallographic directions for $TbMn_2O_5$, $DyMn_2O_5$ and $HoMn_2O_5$. Adapted from [75]. (b) Temperature profile of the polarization for $DyMn_2O_5$ single crystal ($\|b$) at various magnetic fields. The polarization was deduced by the integration of the pyroelectric current in the electric field (200 kV m^{-1}) cooling run. The electric polarization and the applied magnetic field are parallel to the *b* and *a* axes, respectively. Adapted from [79].

for homogeneous long range magnetic order of the antiferromagnetic Mn subsystem and also the Gd magnetic subsystem, possessing a large ferromagnetic moment. In other $REMn_2O_5$ crystals (with nonmagnetic or weakly magnetic rare earth ions) incommensurate or space-modulated magnetic structures in the Mn subsystem are present [78]. The strong Gd–Mn and Gd–Mn–Gd exchange interactions are responsible for the homogeneous magnetic state. A strong effect of the magnetic state on the ferroelectric state in $GdMn_2O_5$ crystal was discovered [80].

Shim *et al* also studied the substitution of Fe and Co at the Mn site of YMn_2O_5. Pure and (Fe, Co) doped YMn_2O_5 series have been successfully prepared by means of the sol–gel process. A similar crystal structure is obtained but very different behaviour patterns are observed depending on the type of the substituents. For example, the parent YMn_2O_5 curve presents a clear increase of the magnetization below 110 K. In the Co and Fe doped $YMn_{2-x}(Fe, Co)_xO_5$ cases, we can see that the saturation magnetizations decrease sharply at low temperature (see figure 11). In addition, the (ferromagnetic) Curie temperature (T_C) increases with doping to $YMn_2O_{5-\delta}$ suggesting that the T_C is higher than room temperature [81] opening the route to practical applications.

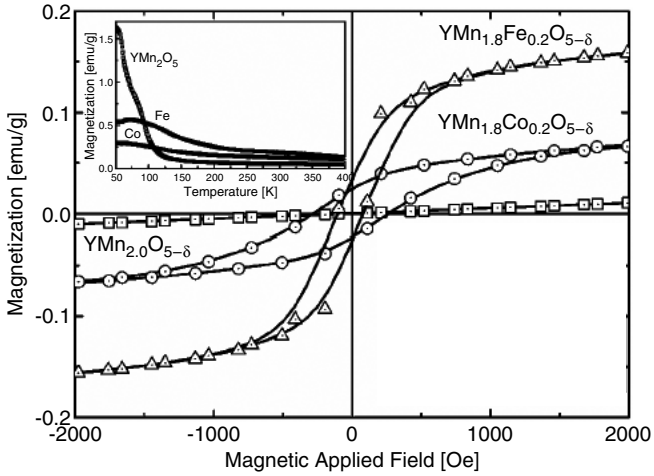

Figure 11. Magnetic hysteresis loop measured by VSM for the polycrystalline $YMn_{2-x}(Fe, Co)_xO_5$ at room temperature. Inset: the temperature dependence of the magnetization. Adapted from [81].

3. Thin films

In view of the practical applications, it is necessary to obtain these materials in the form of thin films. In this section, we review work done to date on multiferroic thin films. For clarity, we have divided this section in two subsections: first, the current work done on single-layer compounds is described whereas in the second subsection, the growth of multicompounds including superlattices and nanocomposites, is presented.

3.1. Single-phase compound

3.1.1. $BiMnO_3$ films. Various deposition techniques (pulsed laser deposition [83–85], spray pyrolysis [19]) have been employed to synthesize $BiMnO_3$ films. For example, $BiMnO_3$ films were grown on (100) Si substrates using nebulized spray pyrolysis by employing manganese (II) acetylacetonate and bismuth (III) acetate as precursors [19]. The 400 nm thick films exhibit a ferromagnetic transition at 105 K (see figure 12) and a ferroelectric transition at around 450 K. They remains ferroelectric down to low temperatures through the ferromagnetic transition [19]. These films on Si substrates are polycrystalline but a preferentially (111) orientation is observed in the out-of-plane direction [85]. In the case of those prepared by pulsed laser deposition on (100) $LaAlO_3$ [85] or (111) $SrTiO_3$ [83, 84], the $BiMnO_3$ films are (100) oriented (see figure 13). Structural analysis by means of x-ray diffraction, electron diffraction and transmission electron microscopy indicated that the films were monoclinic and twinned with two sets of orientation relationships. The first one is (111) $BiMnO_3$ ∥ (100) $SrTiO_3$ and ∼$[\bar{1}01]$ $BiMnO_3$ ∥ ⟨010⟩ $SrTiO_3$; the second one is $(10\bar{1})$ $BiMnO_3$ ∥ (100) $SrTiO_3$ and ∼[121] $BiMnO_3$ ∥ ⟨010⟩ $SrTiO_3$. In pseudocubic notation, the $BiMnO_3$ film is epitaxially aligned cube on cube with the cubic perovskite substrate. The specific orientation relationships described above are due to the monoclinic nature of $BiMnO_3$ which has multiple pseudo-fourfold symmetric planes [86].

The temperature dependence of the magnetization of the $BiMnO_3$ thin films shows a ferromagnetic transition close to 50 K [85] for on $LaAlO_3$ and 97 K [83] for on $SrTiO_3$, lower

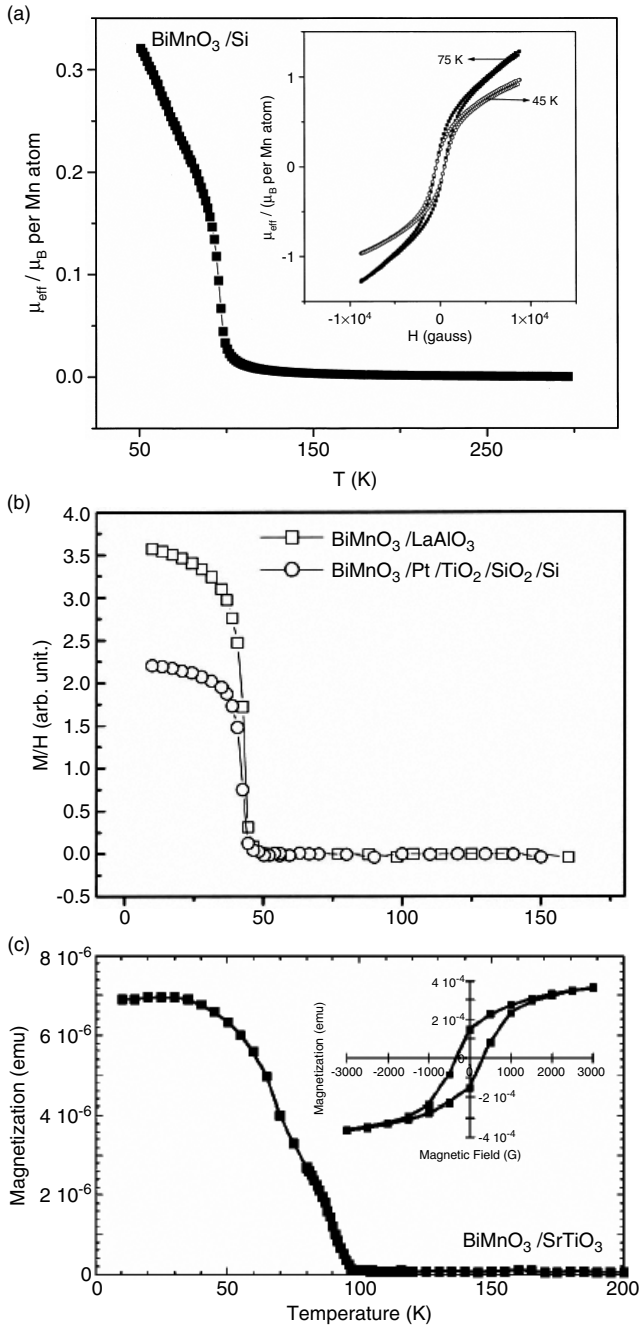

Figure 12. (a) Temperature variation of magnetization of 400 nm $BiMnO_3$ grown on Si at 500 Oe. Inset: the ferromagnetic hysteresis loops measured at 75 and 45 K. From [19]. (b) Temperature dependence of the magnetization of the epitaxial (100) $BiMnO_3$ film and the preferentially (111)-oriented $BiMnO_3$ film (100 nm). Note that the remnant magnetic moment of the epitaxial $BiMnO_3$ thin film on the $LaAlO_3$ substrate is larger than that of the polycrystalline $BiMnO_3$ thin film on the $Pt/TiO_2/SiO_2/Si$ substrate, from [85]. (c) Magnetization curve of the same $BiMnO_3$ film on $SrTiO_3$ cooled under no applied magnetic field. The inset shows the ferromagnetic hysteresis loop at $T = 5$ K. Adapted from [86].

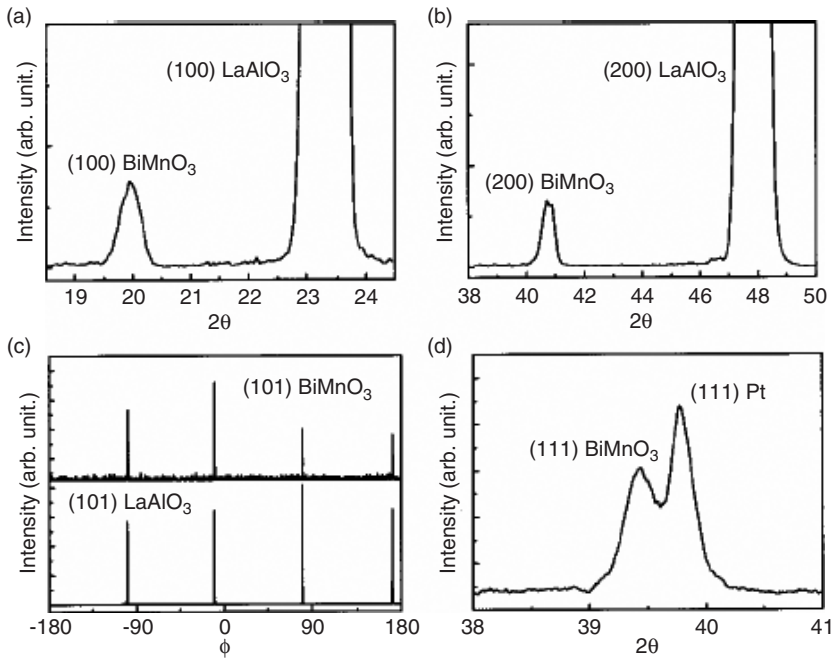

Figure 13. X-ray diffraction pattern of the $BiMnO_3/LaAlO_3$. (a) (100) peak and (b) (200) peak of $BiMnO_3$ thin film. (c) Scan of the (101) peak of the $BiMnO_3$ thin film and (101) peak of the $LaAlO_3$ substrate. (d) The XRD patterns of the (111) peak of the $BiMnO_3$ thin film on the (111) $Pt/TiO_2/SiO_2/Si$ substrate. Adapted from [85].

than that reported by Moreira *et al* [19] (see figure 12). The depression in Curie temperature can be attributed to a nonstoichiometric composition, to strain or to a size effect [86]. The remnant magnetization moment (M_R) of the epitaxial $BiMnO_3$ thin film on the $LaAlO_3$ substrate is larger than that of the polycrystalline $BiMnO_3$ thin film on the $Pt/TiO_2/SiO_2/Si$ substrate, indicating that the magnetic ordering of the epitaxial thin film is better than that of the polycrystalline thin film, similarly to the reports on colossal magnetoresistive thin films [87]. A more interesting result which can be used in relation to the data storage capability is that nanosize bits of ferroelectric polarization on the $BiMnO_3$ thin film on (111) $Pt/TiO_2/SiO_2/Si$ substrate can be easily written and read by a Kelvin force microscope. Moreover, only for the preferentially (111)-oriented $BiMnO_3$ has the ferroelectric polarization been induced at low writing biases, which makes the writing and reading process simple [85].

The optical properties of $BiMnO_3$ films have also been investigated by Sharan *et al*. They report large third-order optical nonlinearities [83] and giant field-induced second-order nonlinearities [84] in thin film which may result from the competition between charge transfer and electron correlation. Moreover, these large second- and third-order optical nonlinearities in $BiMnO_3$ thin films that can be affected by applying external electric fields can potentially lead to interesting device applications.

3.1.2. $BiFeO_3$ films. In this subsection, we will describe the structural properties of the films and then physical properties.

One of the first reports of $BiFeO_3$ films was made by Palkar *et al* [88] on Si substrate using a pulsed laser deposition technique but, recently, a few results have also been reported on

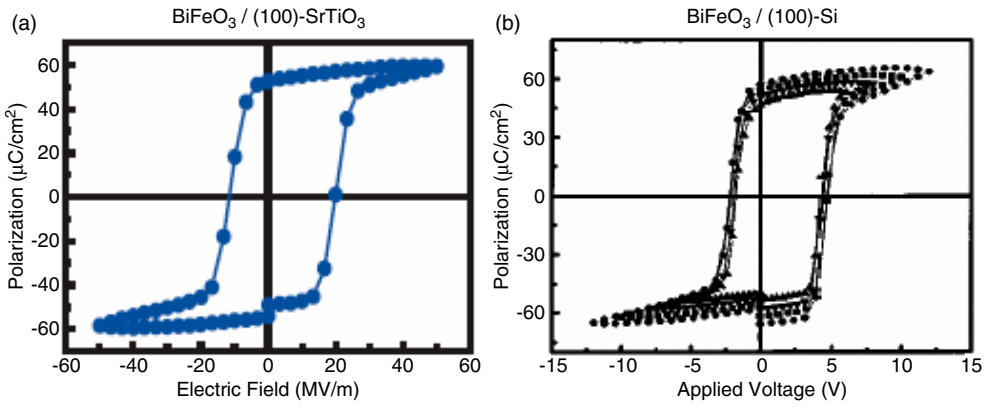

Figure 14. Ferroelectric hysteresis loop for $BiFeO_3$ measured at a frequency of 15 kHz on (a) (100) $SrTiO_3$ substrate and (b) (100) Si substrates. Adapted from [89, 90].

pure $BiFeO_3$ thin films showing both ferroelectricity and ferromagnetism [89]. $BiFeO_3$ thin films were made using the pulsed laser deposition technique on different substrates ($SrTiO_3$, Si). In the case of Si substrate, it is necessary to use a different buffer layer which can be $Pt/TiO_2/SiO_2$ [88] or $SrTiO_3$ as a template layer and $SrRuO_3$ as the bottom electrode [90]. Surprisingly, these earlier authors did not find the same structure of the film: while Wang *et al* found a monoclinic symmetry for on either (100)- or (101)-oriented $SrTiO_3$ substrates (with an in-plane parameter of 3.935 Å and an out-of-plane parameter of 4.0 Å, $c/a = 1.016$ leading to a small distortion of about 0.5°), Yun *et al* obtained a tetragonal structure (space group $P4mm$) for deposition on Si substrates (Palkar *et al* did not established the structure of the film [88]). This is in contrast to the case for bulk material, which is rhombohedral, indicating an effect of the substrate-induced strains. In fact, a rhombohedral structure is obtained only when the films are growing on (111) $SrTiO_3$ substrates [91]. In addition to the substrate, the deposition pressure might also be responsible for the change in the crystal structure [92]. For example, the c axis lattice parameter decreases (4.062–4.006 Å) and the c/a ratio of the films decreases from 1.032 to 1.014 with decrease in the oxygen pressure. The surface roughness and grain size of the films also depend dramatically on the oxygen pressure [92]. The microstructure was also studied [86, 93]. For example, twist distortions about the c axis (to release the shear strain) have been observed [93].

A saturated ferroelectric hysteresis loop is observed for such films [88, 89, 91] indicating a ferroelectric behaviour. The measurement of the polarization of the films gives the most interesting result, as shown by Wang *et al* who observed an enhancement of the spontaneous polarization (P_S) in the strained films [89, 91] (see figure 14). In the case of $SrTiO_3$ substrate, a room temperature spontaneous polarization (50–60 $\mu C\ cm^{-2}$) almost an order of magnitude higher than that of the bulk (6.1 $\mu C\ cm^{-2}$) has been reported [89], higher than the previous report (2.2 $\mu C\ cm^{-2}$) [88]. When the film is grown on Si substrate (using a $SrTiO_3$ template), the spontaneous polarization of the 200 nm thick films was 45 $\mu C\ cm^{-2}$ [90] (see figure 14(b)), also larger than the bulk value. However, this remnant polarization (P_R) of 45 $\mu C\ cm^{-2}$ is smaller than that of films grown on single-crystal $SrTiO_3$ substrates (55 $\mu C\ cm^{-2}$ on (100) $SrTiO_3$ and 95 $\mu C\ cm^{-2}$ on (111) $SrTiO_3$). The higher value for on (111)-oriented substrate is probably due to the fact that a strained, coherent $BiFeO_3$ film on (001) $SrTiO_3$ is very difficult to maintain and (111) $SrTiO_3$ substrates are preferable [93]. Such results confirmed that the stress induced by the substrate strongly influences the ferroelectric properties of

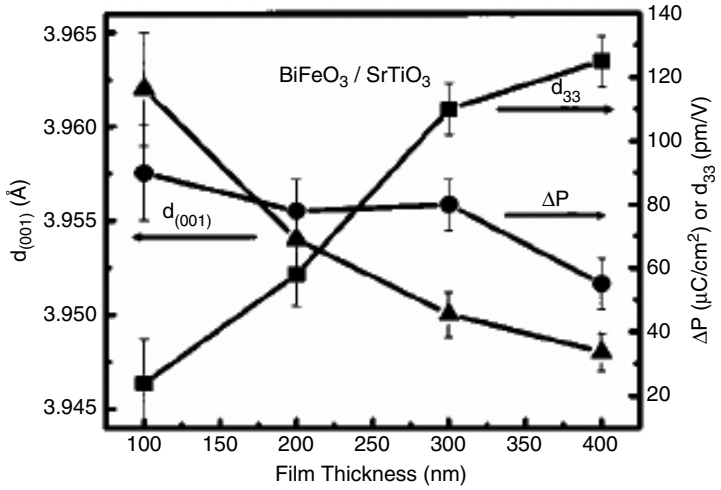

Figure 15. Thickness dependence of the out-of-plane lattice constant (d_{001}), polarization (ΔP) and piezoelectric coefficient (d_{33}) for 200 nm thick $BiFeO_3$ films grown on Si substrates with $SrTiO_3$ as a template layer. Adapted from [90].

the $BiFeO_3$ film. The observed enhancement is corroborated by first-principles calculations and found to originate from a high sensitivity of the polarization to small changes in lattice parameters [89, 94]. Moreover, Bai *et al* evidenced that strains induce a transition between cycloidal and homogeneous antiferromagnetic spin states, releasing a latent antiferromagnetic component locked within the cycloid [95]. However, Palkar *et al* [96] found it difficult to explain the large enhancement in P_S value on the basis of a slight increase in lattice distortion (1.66%); perhaps it is an intrinsic property of the material itself. In order to confirm the strain dependence (inducing lattice distortion), a group at the University of Maryland grew $BiFeO_3$ films on $SrTiO_3$ substrates with various orientations: (001), (101) and (111). The easy axis of spontaneous polarization always lies close to (111), for the various oriented films [91]. This influence of the strains is also confirmed by the enhanced thickness-dependent magnetism compared with that of the bulk [89, 91]. This is evidenced, for Si substrates, in figure 15 where the change in the switchable polarization ΔP is relatively small. On the other hand, the piezoelectric constant d_{33} shows a dramatic increase from $\sim$30 pm V^{-1} for a 100 nm film to $\sim$120 pm V^{-1} for a 400 nm film; the dielectric constant follows the same trend as d_{33}. Note that a similar behaviour for $BiFeO_3$ films grown on $SrTiO_3$ substrates has been reported [89].

In addition to ferroelectricity, the magnetic properties have also been investigated. All films show a well-saturated weak ferromagnetic hysteresis loops at room temperature, with twice the remnant magnetization ($2M_R$), decreasing only slightly with decreasing oxygen pressure [92]. There is a strong dependence of the properties upon the growth conditions. For example, the dielectric constant of the films decreases with decreasing oxygen pressure. The film deposited at 0.05 Torr shows a stable current density and well-saturated hysteresis loop with twice the remnant polarization ($2P_R$) of 136 μC cm^{-2} and a coercive field ($2E_C$) of 109 kV cm^{-1}. The $BiFeO_3$ thin films also show saturated weak ferromagnetic hysteresis loops, in agreement with predictions [97] and a small remnant magnetization ($2M_S = 6$ emu cm^{-3} and $2H_C = 200$ Oe, respectively) [92]. Retention measurement up to several days showed no decay of polarization [90]. Saturated ferroelectric hysteresis loop has been observed in phase-pure and highly resistive $BiFeO_3$ thin films grown on $Pt/TiO_2/SiO_2/Si$ substrates [88]. Study of the

dielectric response of the films with changing temperature indicates an anomaly of the dielectric constant, in the vicinity of Néel temperature (380 °C). This anomaly in temperature is explained by the influence of vanishing magnetic ordering on the electric ordering of magnetoelectric $BiFeO_3$ sample [88].

Enhancements of the ferroelectric and the magnetic properties of $BiFeO_3$ were also obtained by partial substitution of Tb at Bi sites. For example, thin films of the composition $Bi_{0.6}Tb_{0.3}La_{0.1}FeO_3$, integrated on $Si/SiO_2/TiO_2/Pt$ substrate, were fabricated (the ablation was carried out in an oxygen atmosphere of 500 mTorr to maintain oxygen stoichiometry in the film; the substrate was heated to 575 °C during deposition) and display good ferroelectric and magnetic properties and a coupling between them. Though the films are polycrystalline in nature, there is a preferential growth along the $[hk0]$ direction. In pure $BiFeO_3$ thin films, a saturation polarization value of the order of 2.2 μC cm^{-2} is observed, whereas they measured a four-times enhancement in saturation polarization (P_S) in Tb doped thin films [96]. In the present case, since Tb doping in $BiFeO_3$ develops overall ferromagnetism in the sample, the results are independent of the film thickness, in contrast to the reports of Wang *et al* [89]. Thus, the achievement of $BiFeO_3$ thin films with desired magnetoelectric properties, at room temperature when grown on Si substrates, is an important step for applications [90, 96]. Moreover, a piezoelectric coefficient (d_{33}) of ∼60 pm V^{-1} observed in the case of $BiFeO_3$ grown on Si substrates is promising for applications in microelectromechanical systems and actuators [90].

In summary, in these multiferroic materials, a change in the physical properties as compared to the corresponding bulk materials is clearly observed. Such phenomena are common in the case of oxides and have already been reported in manganites for example [87]. In bulk, $BiFeO_3$ crystallized in a rhombohedral distorted perovskite structure whereas in thin films, the structure is sensitive to substrate-induced strains leading to a large polarization. The enhancements of properties of the $BiFeO_3$ films represent a great opportunity and open the route to creating novel devices that can display magnetic and ferroelectric properties [89].

3.1.3. $YMnO_3$ films. Yttrium manganese oxide ($YMnO_3$) exhibits basically two stable crystallographic modifications, orthorhombic and hexagonal. The thermodynamically stable phase under standard synthesis conditions is the hexagonal $YMnO_3$-type one. This has been described in a previous section above. Since this phase is considered as a new candidate for use in nonvolatile memory devices, there is a growing interest in preparing it as a thin film using various deposition techniques, e.g. molecular beam epitaxy [98, 99], laser ablation [100–102] and sputtering [103, 104]. To deposit the $YMnO_3$ films, many substrates have been employed that include (111) MgO, (0001) ZnO:Al/(0001) sapphire and (111) Pt/(111) MgO, Si [105] or (111) Y-stabilized ZrO_2 [106]. Furthermore, its important to note that it is also possible, with an appropriate choice of the substrates, to obtain the orthorhombic structure [106] with either a (010) orientation on $SrTiO_3$ or a (101) orientation on $NdGaO_3$ substrates [52]. To grow the $YMnO_3$ film with the orthorhombic structure, a template layer can also be used [106]. In fact, these studies confirm the competition between the growth of the hexagonal and the orthorhombic $YMnO_3$ phases, the latter being influenced by a strong tensile strain. Such effects where the metastable phases can be stabilized in thin films have been widely utilized in cuprates [107] to synthesize novel phases than can be prepared in the bulk only using extreme conditions such as high pressure.

Fabrication of the hexagonal phase (0001) $YMnO_3$ films on (111) MgO, (0001) ZnO:Al/(0001) sapphire and (111) Pt/(111) MgO have been reported using RF magnetron sputtering [105]. The films are epitaxial only when using (111) MgO, (0001) ZnO:Al/(0001) sapphire [105] or (111) Y-stabilized Y_2O_3 [106] substrates, but are polycrystalline in nature

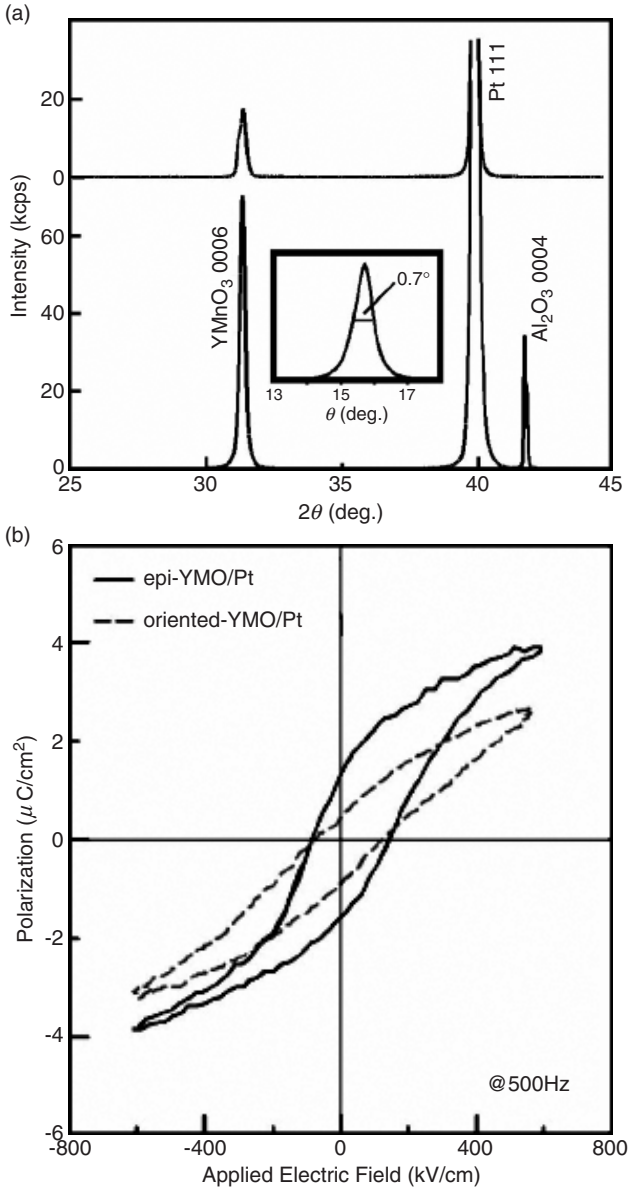

Figure 16. Comparison of the epitaxial $YMnO_3$ the oriented $YMnO_3$ on Pt films. (a) XRD. The inset in the bottom graph corresponds to the rocking curve recorded around the (0006) reflection of the oriented $YMnO_3$. (b) Polarization–electric field (P–E) dependence. Adapted from [108].

on (111) Pt/(111) MgO [105]. Surprisingly this difference does not affect the dielectric properties. Moreover, the dielectric constants of both films are smaller than those reported for $YMnO_3$ single crystal [105]. More recently, the effect of the crystallinity upon the ferroelectric properties of laser ablated $YMnO_3$ films was studied [108]. The epitaxial $YMnO_3$ had much better crystallinity compared to the oriented $YMnO_3$. The full width at half-maxima of the XRD rocking curve, which showed the degree of orientation distribution along [0001] $YMnO_3$ of films, was 0.7° and 1.3° for the epitaxial $YMnO_3$ and the oriented $YMnO_3$, respectively. The ferroelectric properties of epitaxially grown (0001) $YMnO_3$ films on (111) Pt/(0001) sapphire (epitaxial) with an excellent crystallinity were compared to those of (0001)-oriented polycrystalline films on (111)Pt/ZrO_2/SiO_2/Si (see figure 16). From this figure, it is evident

that a ferroelectric-type hysteresis loop was observed in both the structures. The polarization–electric field (P–E) hysteresis of the epitaxial $YMnO_3$ is saturated and the spontaneous polarization (P_S) of 4.0 μC cm^{-2}, the remnant polarization (P_R) of 1.7 μC cm^{-2} and the coercive field (E_C) of 80 kV cm^{-1} are obtained, although the hysteresis is not well defined. In contrast, oriented $YMnO_3$ shows P–E hysteresis without saturation and the P_S, P_R and E_C are 2.8, 0.7 μC cm^{-2}, and 70 kV cm^{-1}, respectively. The E_C of the epitaxial $YMnO_3$ is much higher than that of single crystal (17 kV cm^{-1}) which can probably be explained by the domain pinning caused by the internal defects. A ferroelectric-type capacitance–voltage (C–V) hysteresis loop was also obtained. The C–V hysteresis of the epitaxial $YMnO_3$ on Si substrates is almost identical to the result calculated using the P–E hysteresis of the epitaxial $YMnO_3$ on Pt. A retention time of above 10^4 s at $\pm$15 V with fully polarized ferroelectric domain structure is obtained. The current–voltage (I–V) property is well explained by a Pool–Frenkel-type carrier emission with p-type conduction due to the existence of Mn^{4+} and the activation energy is calculated to be 0.58 eV [110]. These results suggested that the $YMnO_3$ epitaxial films are suitable ferroelectric materials for ferroelectric gate field-effect transistor use [108]. However, the growth temperature might be too high for practical applications (typically 800 °C [108, 110] or 850 °C [111]). To solve this, Choi *et al* suggested modifying $YMnO_3$ by doping Bi at Y sites in order to bring down the processing temperature [111]. They found that highly c-axis-oriented growth of hexagonal $Y_{1-x}Bi_xMnO_3$ films was effective above 5% Bi content modification, at low temperatures (690 °C), without degrading the electrical properties of $YMnO_3$ (such as dielectric constant and leakage current).

In many oxides like manganites, there is a strong effect of the A site cation upon the properties [109]. Thus, Fujimora *et al* have studied the effects of the substitution at the A site upon the dielectric and magnetic properties of $YMnO_3$ films [110]. More precisely, replacement of the Y ion of $YMnO_3$ with other ions such as Mg, Li and Sr has been employed to establish whether there is a carrier concentration effect upon the magnetic properties of $YMnO_3$ films. Although the Li doped sample displays parasitic ferromagnetic behaviour (weak ferromagnetism, probably due to canting of Mn spins), all the films exhibit antiferromagnetic behaviour up to 200 K. The leakage current decreases on substituting Zr for Y and increases on Li or Mg substitution [110]. Thus, the leakage current is critically dependent on the type of metal substitution.

3.2. Artificial multimaterials

3.2.1. Multilayers. The building of artificial lattices makes possible the obtaining of functional materials, because the artificial-lattice technique allows us to combine various kind of compounds and also to introduce lattice strain, low dimensionality and/or interlayer interaction on purpose. Using this technique, new materials such as superconductors [112] have been obtained with a well-controlled structure at the level of the atomic layer [113]. In the present case of multiferroics, the thin film process opens the possibility of tailoring the properties using two different components, one being ferromagnetic and the other being ferroelectric, similarly to the high T_C superconductor case. The aim of this technique is to create materials that display both properties of the parent compounds and their coupling. In fact, in a single-phase compound, the magnetoelectric effect requires long range atomic moments and electric dipoles. For this reason, the effect is often very weak, as observed in the first section of this paper and, as a result, potential applications have not been realized yet. In order to design a compound exhibiting a large effect, van Suchtelen proposed using the product property [114] of the composite. For example, a piezomagnetic phase is mechanically coupled to a piezoelectric phase [115–117]. This effect of coupling mediated by mechanical

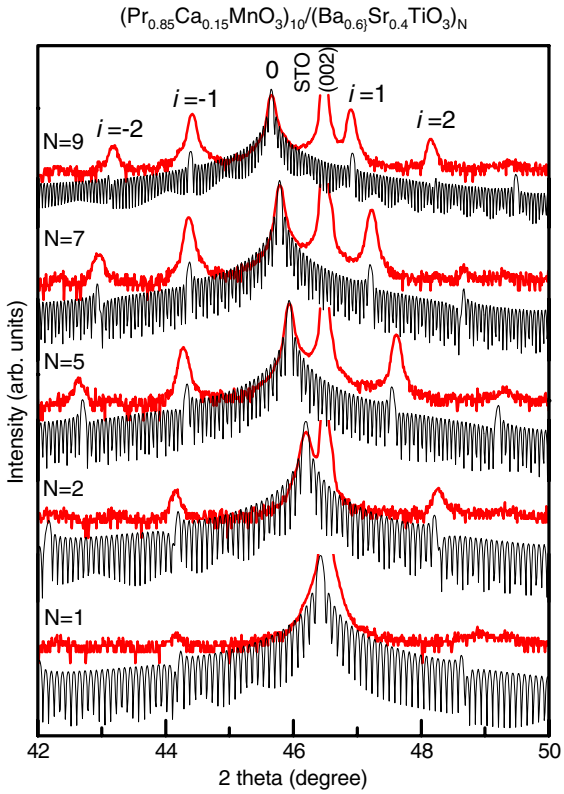

Figure 17. Observed (dark line) and calculated (less dark line) Θ–2Θ XRD scans recorded around the (002) reflection of $SrTiO_3$ substrate for various superlattices $(Pr_{0.85}Ca_{0.15}MnO_3)_{10}/(Ba_{0.6}Sr_{0.4}TiO_3)_N$ ($N = 1$–9). Adapted from [120].

stress at the interface between two phases in a composite has been utilized in order to enhance the magnetoelectric coupling in thin films based on either nanocomposites or superlattices. In this case, by matching a suitable piezomagnetic and an electrostrictive, it might be possible to obtain a large value of the magnetoelectric coefficient.

A series of composition spreads, consisting of ferroelectric $BaTiO_3$ and piezomagnetic $CoFe_2O_4$ layers of varying thicknesses modulated at the nanometre level, were fabricated in order to explore artificial magnetoelectric thin film heterostructures. The composition spread technique offers an efficient way of systematically optimizing the correct ratio in order to obtain the optimal magnetoelectric effect. The properties were investigated at room temperature using scanning microwave microscopy and scanning superconducting quantum interference device microscopy. A map of the dielectric and magnetic properties as a function of the continuously changing average composition across the spreads was obtained. The compositions in the middle of the spreads were found to exhibit ferromagnetism while displaying a dielectric constant as high as 120. The dielectric loss value at 1 GHz was found to vary continuously from 0.2 for the $BaTiO_3$ end to 0.3 for the $CoFe_2O_4$ end for all the spreads (6 nm thick) [118].

The versatility of the pulsed laser deposition technique was also utilized by Murugavel *et al* to create novel artificial structures. Multilayers composed of ferromagnetic $Pr_{0.85}Ca_{0.15}MnO_3$ and ferroelectric $Ba_{0.6}Sr_{0.4}TiO_3$ layers on (100) $SrTiO_3$ substrates were grown [119–121]. High quality superlattices were thus obtained, as seen from the x-ray Θ–2Θ scans (figure 17).

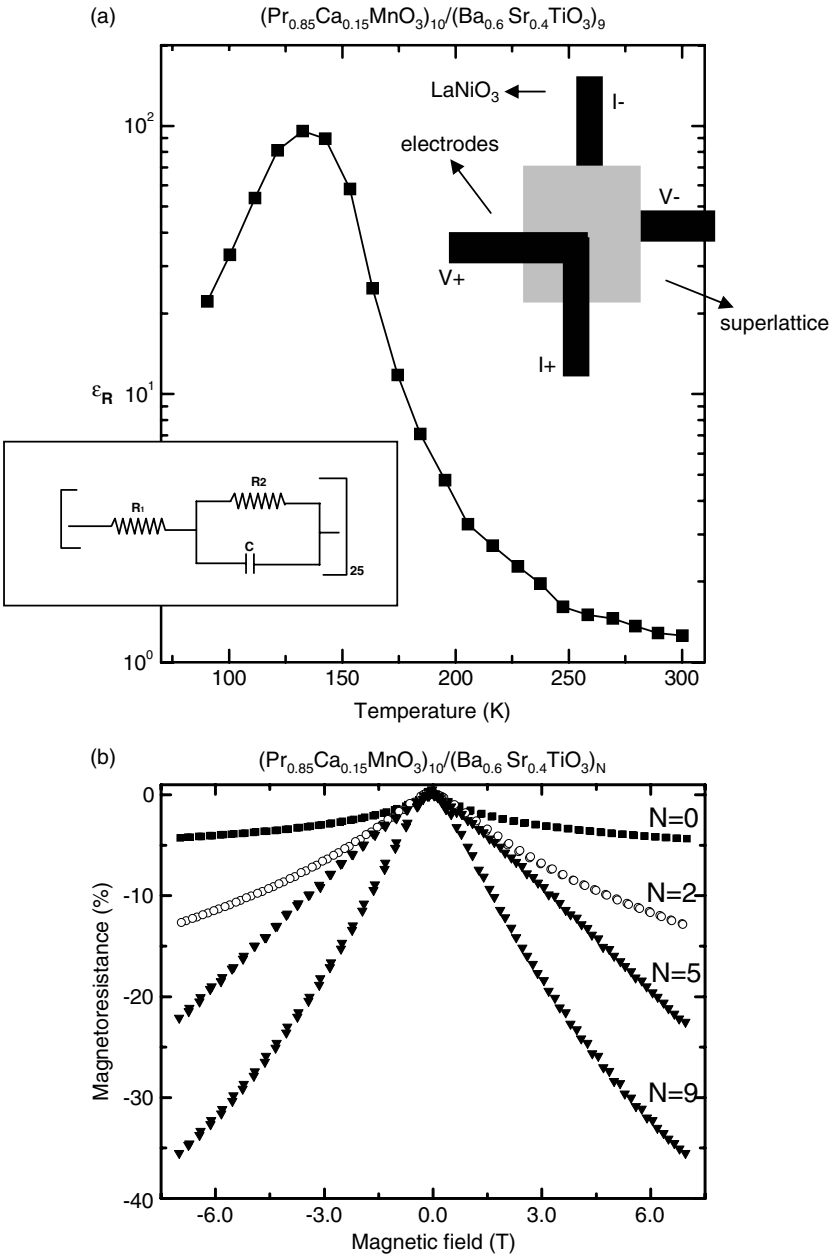

Figure 18. (a) The variation of the dielectric constant and the resistivity with temperature for a $(Pr_{0.85}Ca_{0.15}MnO_3)_{10}/(Ba_{0.6}Sr_{0.4}TiO_3)_9$ sample. The inset shows the junction structure used for the measurement. (b) MR at high magnetic field measured at 100 K for the superlattices $(Pr_{0.85}Ca_{0.15}MnO_3)_{10}/(Ba_{0.6}Sr_{0.4}TiO_3)_N$ with $N = 0$, 2, 5 and 10. In all the measurements, the current is applied perpendicular to the plane of the sample. Adapted from [119].

The dielectric and transport properties of the superlattices were analysed from the complex impedance measurements using a lock-in amplifier. The superlattice with larger ferroelectric thickness shows unique characteristics which are not present for the parent ferromagnetic thin film, such as a peak in the dielectric constant of 100 at 150 K (figure 18(a)) and a

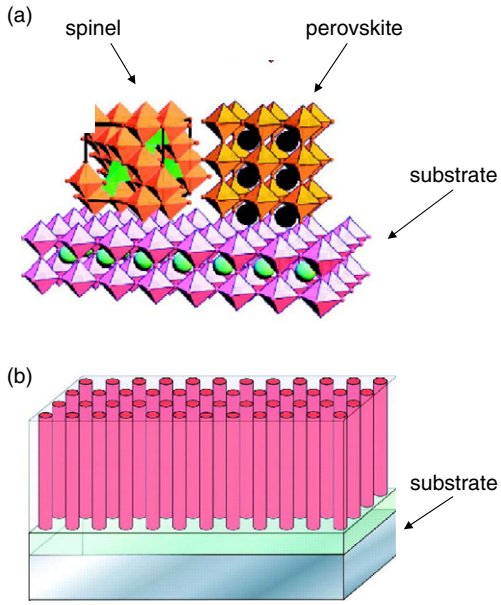

Figure 19. Superlattice of a spinel (top) and a perovskite (middle) on a perovskite substrate (bottom). (B) Schematic illustration of a multilayer structure on a substrate. (C) Epitaxial alignment of a spinel (top left) and a perovskite (top right) on a perovskite substrate (bottom). (D) Schematic illustration of a self-assembled nanostructured thin film formed on the substrate. Adapted from [125].

high magnetoresistance (figure 18(b)). This indicates that those superlattices show both ferromagnetic and ferroelectric transitions which is evidence for the coexistence of both properties, i.e. the formation of a multiferroic material. The high magnetoresistance (40% at 80 K) observed for the superlattice with ten unit cells of $Pr_{0.85}Ca_{0.15}MnO_3$ and nine unit cells of $Ba_{0.6}Sr_{0.4}TiO_3$ can be attributed to the coupling between ferromagnetic and ferroelectric layers, i.e., to the magnetoelectric effect [120]. This is confirmed by the recent work of Singh *et al* on a $La_{0.7}Ca_{0.3}MnO_3/BaTiO_3$ superlattice, where the magnetic properties are strongly dependent on the ferroelectric $BaTiO_3$ thickness [122]. The AC electrical studies also reveal that the impedance and capacitance in these films vary with the applied magnetic field due to the magnetoelectrical coupling in these structures—a key feature of multiferroics—and magnetocapacitance is also observed. In the same way, it will be interesting to build a superlattice made of $BiFeO_6$ and $BiCrO_6$ compounds using (111) $SrTiO_3$ substrates (similarly to in the work of Ueda *et al* [123], where they synthesized a new ferromagnetic material based on antiferromagnetic compounds) since, on the basis of first-principles density functional theory, the polarization, piezoelectric coefficient and magnetization should be higher than those for all known multiferroics [124]. This approach is promising if one can find phases where the interfacial strain is reduced, keeping the substrate-induced strain low. Thus, in order to avoid the effect of the substrate, it is necessary to grow the film such in a way that the stress along the out-of-plane direction is reduced. The use of nanocomposites is a possible direction that has also been utilized in a similar way to that of bulk, previously [114].

3.2.2. Nanocomposites films. To produce multiferroic thin films, Zheng *et al* used a different approach [125, 126]. Instead of trying to produce a single compound as is done

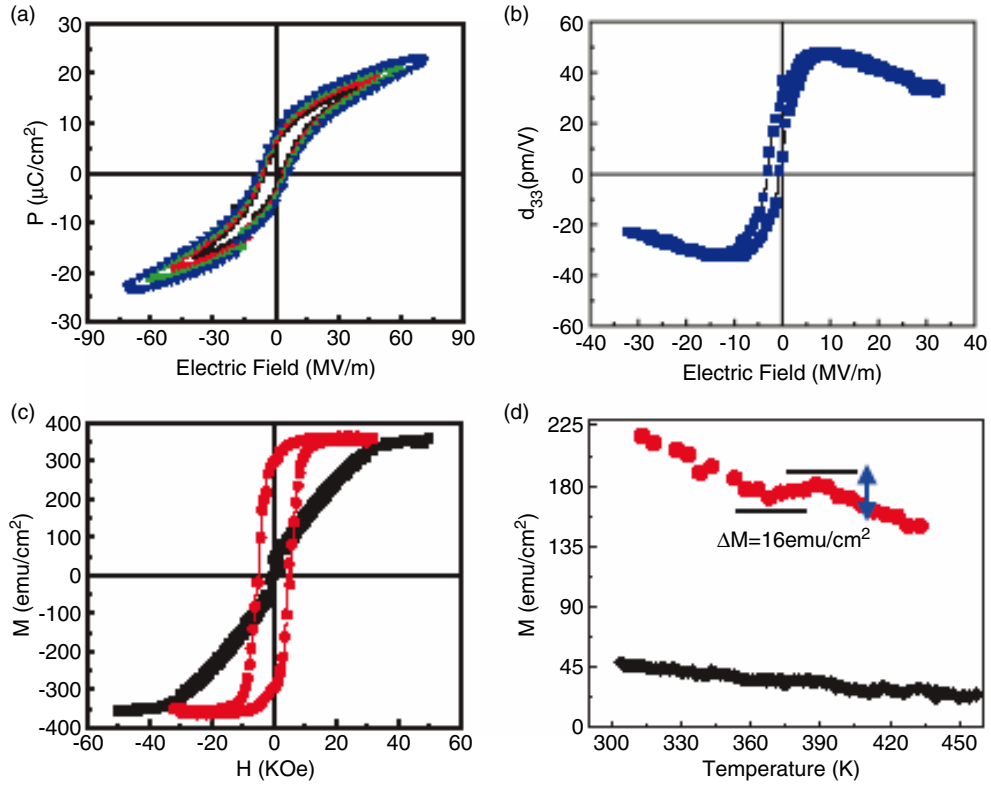

Figure 20. (a) Polarization electric field hysteresis loop showing that the film is ferroelectric with a saturation polarization $P_S = 23\ \mu C\ cm^{-2}$. (b) Small signal piezoelectric d_{33} hysteresis loop for a 50 m diameter capacitor. (c) Out-of-plane (red) and in-plane (black) magnetic hysteresis loops showing the large uniaxial anisotropy. (d) Magnetization versus temperature curve measured under 100 Oe, which shows a distinct drop in magnetization at the ferroelectric Curie temperature for the vertically self-assembled nanostructure (red curve); the multilayered nanostructure (black curve) shows negligible change in magnetization. Adapted from [125].

in the classical way, they grew a composite material from magnetic cobalt ferrite ($CoFe_2O_4$ which is ferrimagnetic with large magnetostriction) and ferroelectric barium titanate ($BaTiO_3$ which is ferroelectric with large piezoelectricity) on a substrate. Such nanostructures are deposited on (100) $SrTiO_3$ substrates by the pulsed laser deposition technique from a single $0.65BaTiO_3$–$0.35CoFe_2O_4$ target. They found using x-ray and electron diffractions that the films are epitaxial in the plane as well as out of the plane, with self-assembled hexagonal arrays of $CoFe_2O_4$ nanopillars embedded in a $BaTiO_3$ matrix, giving a clear example of a 3D heteroepitaxy (figure 19). Surprisingly, spinel $CoFe_2O_4$ and perovskite $BaTiO_3$ phases spontaneously separated during heteroepitaxial growth [126]. Arrays of $CoFe_2O_4$ nanopillars with both diameters and average spacings of about 20–30 nm formed in a $BaTiO_3$ matrix as seen from transmission electron microscopy. As the substrate temperature increases from 750 to 950 °C, the average diameter of the pillars increases from 9 to 70 nm. The temperature-dependent magnetic measurements illustrate the coupling between the two order parameters, which is manifested as a change in magnetization at the ferroelectric Curie temperature (figure 20). They claimed, on the basis of thermodynamic analyses, that the magnetoelectric coupling in such a nanostructure can be understood on the basis of the strong elastic interactions

between the two phases. In fact, the coupling between ferroelectric and magnetic order parameters facilitates the interconversion of energies stored in electric and magnetic fields which will be useful for device applications (energy transducers and field sensors for example). In comparison to the superlattice case, the mechanical coupling in these nanostructures is probably much stronger due to this epitaxial matching in the three directions.

4. Conclusion

A few compounds, naturally existing or artificially created, have been revealed to be multiferroic and have become a topic of great interest during recent years. The most challenging related task is searching for new compounds which behave as multiferroics. In reviewing growth and properties of multiferroics, issues of creating new materials and understanding the origin of multiferroism in them and the mechanism of the coupling between ferroelectric and magnetic domains are seen as the most challenging aspects. Now, it will be worth reviewing the work on layered materials and nanocomposites, which has also undergone significant developments in the past few years, but which is beyond the scope of the present article. There is no doubt in our minds that in the forthcoming years, multiferroics will be a topic of great interest, both in science and technology, because of their interesting properties and their offering a new dimensionality for novel devices.

Acknowledgments

We thank Professor B Raveau, Dr Ch Simon, Professor B Mercey for helpful discussions.

This review was carried out in the framework of the Work Package 'New Architectures for Passive Electronics of the European Network of Excellence' 'Functional Advanced Materials Engineering of Hybrids and Ceramics' FAME (FP6-500159-1) supported by the European Community and by Centre National de la Recherche Scientifique. Financial support was also provided by the Centre Franco-Indien pour la Promotion de la Recherche Avancee/Indo-French Centre for the Promotion of Advanced Research (CEFIPRA/IFCPAR) under Project No 2808-1. One of us acknowledges the Ministère de la Jeunesse et de l'Education Nationale for his fellowship (2003/87).

References

[1] Garcia N, Munoz M and Zhao Y-W 1999 *Phys. Rev. Lett.* **82** 2923
[2] Gabureac M, Viret M, Ott F and Fermon C 2004 *Phys. Rev.* B **69** 100401(R)
[3] Ascher E, Rieder H, Schmid H and Stossel H 1966 *J. Appl. Phys.* **37** 1404
[4] Gregg J F, Petej I, Jouguelet E and Dennis C 2002 *J. Phys. D: Appl. Phys.* **35** R121
[5] Schmid H 1994 *Ferroelectrics* **162** 317
[6] For a review on the magnetoelectric effect see Fiebig M 2005 *J. Phys. D: Appl. Phys.* **38** R123
[7] Ascher E, Rieder H, Schmid H and Stössel H 1966 *J. Appl. Phys.* **37** 1404
[8] Smolensky G A, Agranovskaya A I and Isupov V A 1959 *Sov. Phys.—Solid State* **1** 149
[9] Smolensky G A, Isupov V A, Krainik N N and Agranovskaya A I 1961 *Isv. Akad. Nauk SSSR, Ser Fiz.* **25** 1333
[10] Brixel W, Rivera J P, Steiner A and Schmid H 1988 *Ferroelectrics* **79** 201
[11] Astrov D N, Alshin B I, Tomashpolski Y Y and Venevtsev Y N 1969 *Sov. Phys.—JETP* **28** 1123
[12] Drobyshev L A, Alshin B I, Tomashpolski Y Y and Venevtsev Y N 1970 *Sov. Phys.—Crystallogr.* **14** 634
[13] Cai N, Zhai J, Nan C W, Lin Y and Zhi Z 2003 *Phys. Rev.* B **68** 224103
[14] Zeng M, Wan J G, Wang Y, Yu H, Liu J-M, Jiang X P and Nan C W 2004 *J. Appl. Phys.* **95** 8069
[15] Liu Y X, Wan J G, Liu J-M and Nan C W 2003 *J. Appl. Phys.* **94** 5118
[16] Filippetti A and Hill N A 2002 *Phys. Rev.* B **65** 195120
[17] Hill N A and Rabe K M 2000 *AIP Conf. Proc.* **535** 372
[18] Hill N A and Rabe K M 1999 *Phys. Rev.* B **59** 8759

[19] Moreira dos Santos A, Parashar S, Raju A R, Zhao Y S, Cheetham A K and Rao C N R 2002 *Solid State Commun.* **122** 49
[20] Bokov V A, Myl'nikova I E, Kizhaev S A, Bryzhina M F and Grigoryan N A 1966 *Sov. Phys.—Solid State* **7** 2993
[21] Sugawara F, Ida S, Syono Y and Akimoto S 1968 *J. Phys. Soc. Japan* **25** 1553
[22] Atou T, Chiba H, Ohoyama K, Yamaguchi Y and Syono Y 1999 *J. Solid State Chem.* **145** 639
[23] Moreira dos Santos A, Cheetham A K, Atou T, Syono Y, Yamaguchi Y, Ohoyama K, Chiba H and Rao C N R 2002 *Phys. Rev.* B **66** 064425
[24] Seshadri R and Hill N A 2001 *Chem. Mater.* **13** 2892
[25] Rao C N R, Arulraj A, Cheetham A K and Raveau B 2000 *J. Phys.: Condens. Matter* **12** R83
[26] Shishidou T, Mikano N, Uratani Y, Ishii F and Oguchi T 2004 *J. Phys.: Condens. Matter* **16** S5677
[27] Kimura T, Kawamoto S, Yamada Y, Azuma M, Takano M and Tokura Y 2003 *Phys. Rev.* B **67** 180401(R)
[28] Zhong C G, Fang J H and Jiang Q 2004 *J. Phys.: Condens. Matter* **16** 9059
[29] Gehring G A 1994 *Ferroelectrics* **161** 275
[30] Goodenough J B and Longo 1978 *Landolt–Börnstein New Series* Group III/vol 4a (New York: Springer)
[31] Palkar V R, Kundaliya D C and Malik S K 2003 *J. Appl. Phys.* **93** 4337
[32] Sosnowska I, Peterlin-Neumaier T and Steichele E 1982 *J. Phys. C: Solid State Phys.* **15** 4835
[33] Mahesh Kumar M, Palkar V R, Srinivas K and Suryanarayana S V 2000 *Appl. Phys. Lett.* **76** 2764
[34] Bucci J D, Robertson B K and James W J 1972 *J. Appl. Crystallogr.* **5** 187
[35] Kubel F and Schmid H 1990 *Acta Crystallogr.* B **46** 698
[36] Smolenskii G A 1982 *Sov. Phys.—Usp.* **25** 475
[37] Wang Y P, Zhou L, Zhang M F, Chen X Y, Liu J M and Liu Z G 2004 *Appl. Phys. Lett.* **84** 1731
[38] Mathe V L, Patankar K K, Patil R N and Lokhande C D 2004 *J. Magn. Magn. Mater.* **270** 380
[39] Palkar V R, Kundaliya D C, Malik S K and Bhattacharya S 2004 *Phys. Rev.* B **69** 212102
[40] Hill N A and Filippetti A 2002 *J. Magn. Magn. Mater.* **242–245** 976
[41] Hill N A 2000 *J. Phys. Chem.* B **104** 6694
[42] Vickery R C and Klann A 1957 *J. Chem. Phys.* **27** 1161
[43] Belov K P, Zaitseva M A and Pedko A V 1959 *J. Exp. Theor. Phys.* **36** 1672
[44] Yakel H L, Koehler W C, Bertaut E F and Forrat E F 1963 *Acta Crystallogr.* **16** 957
[45] Bertaut E F and Forrat F 1956 *J. Phys. Radium* **20** 404
[46] Bertaut E F, Forrat F and Fang P H 1963 *C. R. Acad. Sci.* **256** 1958
[47] Van Aken B B, Meetsma A and Palstra T T M 2001 *Acta Crystallogr.* E **57** 38
[48] Van Aken B B, Meetsma A and Palstra T T M 2001 *Acta Crystallogr.* E **57** 101
[49] Abrahams S C 2001 *Acta Crystallogr.* B **57** 485
[50] Kajimoto R, Yoshizawa H, Shintani H, Kimura T and Tokura Y 2004 *Phys. Rev.* B **70** 012401
[51] Van Aken B B, Meetsma A and Palstra T T M 2001 *Acta Crystallogr.* E **57** 87
[52] Salvador P A, Doan T D, Mercey B and Raveau B 1998 *Chem. Mater.* **10** 2593
[53] Galasso F S 1968 *Structure Properties and Preparation of Perovskite-Type Compounds* (Oxford: Pergamon)
[54] Carp O, Patron L, Ianculescu A, Pasuk J and Olar R 2000 *J. Alloys Compounds* **351** 314
[55] Lonkai Th, Tomuta D G, Amann U, Ihringer J, Hendrikx R W A, Többens D M and Mydosh J A 2004 *Phys. Rev.* B **69** 134108
[56] Lonkai Th, Tomuta D G, Hoffmann J-U, Schneider R, Hohlwein D and Ihringer J 2004 *J. Appl. Phys.* **93** 8191
[57] Medvedeva J E, Anisimov V I, Korotin M A, Mryasov O N and Freeman A J 2000 *J. Phys.: Condens. Matter* **12** 4947
[58] Huang Z J, Cao Y, Sun Y Y, Xue Y Y and Chu C W 1997 *Phys. Rev.* B **56** 2623
[59] Fiebig M, Lottermoser Th, Fröhlich D, Goltsev A V and Pisarev R V 2002 *Nature* **419** 818
[60] Lottermoser Th and Fiebig M 2004 *Phys. Rev.* B **70** 220407(R)
[61] Van Aken B B, Palstra T T M, Filipetti A and Spaldin N A 2004 *Nat. Mater.* **3** 164
[62] Fröhlich D, Leute St, Pavlov V V, Pisarev R V and Kohn K 1999 *J. Appl. Phys.* **85** 4762
[63] Fiebig M, Fröhlich D, Kohn K, Leute St, Lottermoser Th, Pavlov V V and Pisarev R V 2000 *Phys. Rev. Lett.* **84** 5620
[64] Sharma P A, Ahn J S, Hur N, Park S, Kim S-B, Lee S, Park J-G, Guha S and Cheong S-W 2004 *Phys. Rev. Lett.* **93** 1770202
[65] Lorenz B, Litvinchuk A P, Gospodinov M M and Chu C W 2004 *Phys. Rev. Lett.* **92** 087204
[66] Lorenz B, Wang Y Q, Sun Y Y and Chu C W 2004 *Phys. Rev.* B **70** 212412
[67] Goto T, Kimura T, Lawes G, Ramirez A P and Tokura Y 2004 *Phys. Rev. Lett.* **92** 257201
[68] Kajimoto R, Yoshizawa H, Shintani H, Kimura T and Tokura Y 2004 *Phys. Rev.* B **70** 012401

[69] Kimura T, Goto T, Thizaka K, Arima T and Tokura Y 2003 *Nature* **426** 55
[70] Schouchkov A B, Simpson J R, Quijada M, Ishibashi H, Hur N, Ahn J S, Cheong S W, Millis A J and Drew H D 2003 *Phys. Rev. Lett.* **91** 027203
[71] Van Aken B B and Palstra T T M 2004 *Phys. Rev.* B **69** 134113
[72] Quezel-Ambrunaz S, Bertaut E F and Buisson G 1964 *C. R. Acad. Sci.* **258** 3025
[73] Bertaut E F, Buisson G, Durif A, Mareschal A, Montmory M C and Quezel-Ambrunaz S 1965 *Bull. Soc. Chim. Fr.* 1132
[74] Hur N, Park S, Sharma P A, Ahn J S, Guha S and Cheong S-W 2004 *Nature* **429** 392
[75] Hur N, Park S, Sharma P A, Guha S and Cheong S W 2004 *Phys. Rev. Lett.* **93** 107207
[76] Alonso J A, Casaos M R T, Martinez-Lope M J and Rasines I 1997 *J. Solid State Chem.* **129** 105
[77] Abrahams S C and Bernstein J L 1967 *J. Chem. Phys.* **46** 3776
[78] Chapon L C, Blake G R, Gutmann M J, Park S, Hur N, Radaelli P G and Cheong S-W 2004 *Phys. Rev. Lett.* **93** 177402
[79] Higashiyama D, Miyasaka S, Kida N, Arima T and Tokura Y 2004 *Phys. Rev.* B **70** 174405
[80] Golovenchits E and Sanina V 2004 *J. Phys.: Condens. Matter* **16** 4325
[81] Shim I-B, Yeom J H, Choi K R, Kim C S, Shin H J and An S Y 2004 *J. Appl. Phys.* **95** 7070
[82] Kagomiya I, Kohn K and Uchiyama T 2002 *Ferroelectrics* **280** 297
[83] Sharan A, An I, Chen C, Collins R W, Lettieri J, Jia Y, Schlom D G and Gopalan V 2003 *Appl. Phys. Lett.* **83** 5169
[84] Sharan A, Lettieri J, Jia Y, Tian W, Pan X, Schlom D G and Gopalan V 2004 *Phys. Rev.* B **69** 214109
[85] Son J Y, Kim B G, Kim C H and Cho J H 2004 *Appl. Phys. Lett.* **84** 4971
[86] Moreira dos Santos A F, Cheetham A K, Tian W, Pan X, Jia Y, Murphy N J, Lettieri J and Schlom D G 2004 *Appl. Phys. Lett.* **84** 91
[87] Prellier W, Lecoeur Ph and Mercey B 2001 *J. Phys.: Condens. Matter* **13** R915
[88] Palkar V R, John J and Pinto R 2002 *Appl. Phys. Lett.* **80** 1628
[89] Wang J, Neaton J B, Zheng H, Nagarajan V, Ogale S B, Liu B, Viehland D, Vaithyanathan V, Schlom D G, Waghmare U V, Spaldin N A, Rabe K M, Wuttig M and Ramesh R 2003 *Science* **299** 1719
[90] Wang J, Zheng H, Ma Z, Prasertchoung S, Wuttig M, Droopad R, Yu J, Eisenbeiser K and Ramesh R 2003 *Appl. Phys. Lett.* **85** 2574
[91] Li J, Wang J, Wuttig M, Ramesh R, Wang N, Ruette B, Pyatakov A P, Zvezdin A K and Viehland D 2004 *Appl. Phys. Lett.* **84** 5261
[92] Yun K Y, Noda M, Okuyama M, Saeki H, Tabata H and Saito K 2004 *J. Appl. Phys.* **96** 3399
[93] Qi X, Wei M, Lin Y, Jia Q, Zhi D, Dho J, Blamire M G and MacManus-Driscoll J L 2005 *Appl. Phys. Lett.* **86** 071914
[94] Edeter C and Spaldin N A 2005 *Preprint* cond-mat/0502364v1
[95] Bai F, Wang J, Wuttig M, Li J F, Wang N, Pyatakov A P, Zvezdin A K, Cross L E and Viehland D 2005 *Appl. Phys. Lett.* **86** 032511
[96] Palkar V R, Ganesh Kumara K and Malik S K 2004 *Appl. Phys. Lett.* **84** 2856
[97] Edeter C and Spaldin N A 2005 *Phys. Rev.* B **71** 060401(R)
[98] Imada S, Shouriki S, Tokumitsu E and Ishiwara H 1998 *Japan. J. Appl. Phys.* **37** 6497
[99] Imada S, Kuraoka T, Tokumitsu E and Ishiwara H 2001 *Japan. J. Appl. Phys.* **40** 666
[100] Ito D, Fujimura N, Yoshimura T and Ito T 2003 *J. Appl. Phys.* **94** 4036
[101] Ito D, Fujimura N and Ito T 2000 *Japan. J. Appl. Phys.* **39** 5525
[102] Yoshimura T, Fujimura N and Ito T 1998 *Appl. Phys. Lett.* **73** 414
[103] Yoshimura T, Fujimura N, Ito D and Ito T 1996 *J. Appl. Phys. Lett.* **80** 7084
[104] Lee H N, Kim Y T and Park Y K 1999 *Appl. Phys. Lett.* **74** 3887
[105] Fujimura N, Ishida T, Yoshimura T and Ito T 1996 *Appl. Phys. Lett.* **69** 1011
[106] Dho J, Leung C W, MacManus-Driscoll J L and Blamire M G 2004 *J. Cryst. Growth* **267** 548
[107] Mercey B, Salvador P A, Prellier W, Doan T D, Wolfman J, Hamet J F, Hervieu M and Raveau B 1999 *J. Mater. Chem.* **9** 233
[108] Ito D, Fujimura N, Yoshimura T and Ito T 2003 *J. Appl. Phys.* **93** 5663
[109] Sundaresan A, Maignan A and Raveau B 1997 *Phys. Rev.* B **56** 5092
[110] Fujimura N, Sakata H, Ito D, Yoshimura T, Yokota T and Ito T 2003 *J. Appl. Phys.* **93** 6990
[111] Choi T and Lee J 2004 *Appl. Phys. Lett.* **84** 5043
[112] Prellier W, Mercey B, Lecoeur Ph, Hamet J F and Raveau B 1997 *Appl. Phys. Lett.* **71** 782
[113] Mercey B, Salvador P A, Lecoeur Ph, Prellier W, Hervieu M, Simon Ch, Chippaux D, Haghiri-Gosnet A M and Raveau B 2003 *J. Appl. Phys.* **94** 2716
[114] van Suchtelen J 1972 *Philips Res. Rep.* **27** 28

[115] van de Boomgaard J, Terell D R and Born R A J 1974 *J. Mater. Sci.* **9** 1705
[116] van de Boomgaard J and Born R A J 1978 *J. Mater. Sci.* **13** 1538
[117] van de Boomgaard J, van Run A M J G and van Suchtelen J 1976 *Ferroelectrics* **14** 727
[118] Chang K S, Aronova M A, Lin C-L, Murakami M, Yu M H, Hattrick-Simpers J, Famodu O O, Lee S Y, Ramesh R, Wuttig M, Takeuchi I, Gao C and Bendersky L A 2004 *Appl. Phys. Lett.* **84** 3091
[119] Murugavel P, Saurel D, Prellier W, Simon Ch and Raveau B 2004 *Appl. Phys. Lett.* **85** 4424
[120] Murugavel P, Padhan P and Prellier W 2004 *Appl. Phys. Lett.* **85** 4992
[121] Murugavel P, Singh M P, Prellier W, Mercey B, Simon Ch and Raveau B 2005 *J. Appl. Phys.* **97** 103914
[122] Singh M P, Prellier W, Simon Ch and Raveau B 2005 *Appl. Phys. Lett.* **87** 022505
[123] Ueda K, Tabata H and Kawai T 1998 *Science* **290** 1064
[124] Baettig P and Spaldin N A 2005 *Appl. Phys. Lett.* **86** 012505
[125] Zheng H, Wang J, Lofland S E, Ma Z, Mohaddes-Ardabili L, Zhao T, Salamanca-Riba L, Shinde S R, Ogale S B, Bai F, Viehland D, Jia Y, Schlom D G, Wuttig M, Roytburd A and Ramesh R 2004 *Science* **303** 661
[126] Zheng H, Wang J, Mohaddes-Ardabili L, Wuttig M, Salamanca-Riba L, Schlom D G and Ramesh R 2004 *Appl. Phys. Lett.* **85** 2035